# Inverse estimates of the oceanic sources and sinks of natural $CO_2$ and the implied oceanic carbon transport

S. E. Mikaloff Fletcher,[1,2] N. Gruber,[1,3] A. R. Jacobson,[4,5] M. Gloor,[4,6] S. C. Doney,[7] S. Dutkiewicz,[8] M. Gerber,[9] M. Follows,[8] F. Joos,[9] K. Lindsay,[10] D. Menemenlis,[11] A. Mouchet,[12] S. A. Müller,[9] and J. L. Sarmiento[4]

[1]   We use an inverse method to estimate the global-scale pattern of the air-sea flux of natural $CO_2$, i.e., the component of the $CO_2$ flux due to the natural carbon cycle that already existed in preindustrial times, on the basis of ocean interior observations of dissolved inorganic carbon (*DIC*) and other tracers, from which we estimate $\Delta C_{gasex}$, i.e., the component of the observed *DIC* that is due to the gas exchange of natural $CO_2$. We employ a suite of 10 different Ocean General Circulation Models (OGCMs) to quantify the error arising from uncertainties in the modeled transport required to link the interior ocean observations to the surface fluxes. The results from the contributing OGCMs are weighted using a model skill score based on a comparison of each model's simulated natural radiocarbon with observations. We find a pattern of air-sea flux of natural $CO_2$ characterized by outgassing in the Southern Ocean between 44°S and 59°S, vigorous uptake at midlatitudes of both hemispheres, and strong outgassing in the tropics. In the Northern Hemisphere and the tropics, the inverse estimates generally agree closely with the natural $CO_2$ flux results from forward simulations of coupled OGCM-biogeochemistry models undertaken as part of the second phase of the Ocean Carbon Model Intercomparison Project (OCMIP-2). The OCMIP-2 simulations find far less air-sea exchange than the inversion south of 20°S, but more recent forward OGCM studies are in better agreement with the inverse estimates in the Southern Hemisphere. The strong source and sink pattern south of 20°S was not apparent in an earlier inversion study, because the choice of region boundaries led to a partial cancellation of the sources and sinks. We show that the inversely estimated flux pattern is clearly traceable to gradients in the observed $\Delta C_{gasex}$, and that it is relatively insensitive to the choice of OGCM or potential biases in $\Delta C_{gasex}$. Our inverse estimates imply a southward interhemispheric transport of $0.31 \pm 0.02$ Pg C yr$^{-1}$, most of which occurs in the Atlantic. This is considerably smaller than the 1 Pg C yr$^{-1}$ of Northern Hemisphere uptake that has been inferred from atmospheric $CO_2$ observations during the 1980s and 1990s, which supports the hypothesis of a Northern Hemisphere terrestrial sink.

[1]Department of Atmospheric and Oceanic Sciences and Institute of Geophysics and Planetary Physics, University of California, Los Angeles, California, USA.

[2]Now at Atmospheric and Oceanic Sciences, Princeton University, Princeton, New Jersey, USA.

[3]Now at Environmental Physics, Institute of Biochemistry and Pollutant Dynamics ETH Zürich, Zurich, Switzerland.

[4]Atmospheric and Oceanic Sciences, Princeton University, Princeton, New Jersey, USA.

[5]Now at NOAA Earth System Research Laboratory, Global Monitoring Division, Boulder, Colorado, USA.

[6]Now at Institutes of Earth and Biosphere, Energy and Environment and School of Geography, University of Leeds, Leeds, UK.

[7]Marine Chemistry and Geochemistry, Woods Hole Oceanographic Institution, Woods Hole, Massachusetts, USA.

[8]Department of Earth, Atmosphere, and Planetary Sciences, Massachusetts Institute of Technology, Cambridge, Massachusetts, USA.

[9]Climate and Environmental Physics, Physics Institute, University of Bern, Bern, Switzerland.

[10]Climate and Global Dynamics Division, National Center for Atmospheric Research, Boulder, Colorado, USA.

[11]Estimating the Circulation and Climate of the Ocean, Jet Propulsion Laboratory, Pasadena, California, USA.

[12]Astrophysics and Geophysics Institute, University of Liege, Liege, Belgium.

## 1. Introduction

[2] The air-sea exchange of CO$_2$ is a major determinant of the spatial and temporal distribution of atmospheric CO$_2$, which is used to draw major conclusions about the global carbon cycle [*Keeling et al.*, 1989b; *Tans et al.*, 1990; *Gurney et al.*, 2002]. The contemporary air-sea flux of CO$_2$ can be broken down into two primary components: the exchange of natural CO$_2$ that existed in preindustrial times and the uptake of anthropogenic CO$_2$, which is driven by the perturbation of atmospheric CO$_2$ by fossil fuel burning, cement production, and land use change [*Sarmiento et al.*, 1992; *Murnane et al.*, 1999; *Gruber and Sarmiento*, 2002]. A potential additional component is the perturbation flux of CO$_2$ that arises owing to changes in ocean circulation and ocean biology as a consequence of climate change [*Sarmiento et al.*, 1998; *Matear and Hirst*, 1999; *Joos et al.*, 1999; *Gruber et al.*, 2004]. Model simulations indicate that this flux is still relatively small compared to the other two flux components [e.g., *Plattner et al.*, 2001], but will become more important later in this century.

[3] Separate estimates of the natural and anthropogenic air-sea flux help elucidate the processes driving these air-sea fluxes and are critical to interpreting the contemporary spatial and temporal gradients in atmospheric CO$_2$ in terms of carbon sources and sinks. In particular, natural carbon transport in the interior ocean has played a major role in discussions about the processes responsible for the Northern Hemisphere carbon sink that is implied by the latitudinal gradient of atmospheric CO$_2$ during the 1980's and 1990's, which is smaller than expected on the basis of the anthropogenic CO$_2$ emission pattern [e.g., *Keeling et al.*, 1989b; *Tans et al.*, 1990]. *Keeling et al.* [1989b] suggested that this Northern Hemisphere carbon sink is due to an uptake of about 1 Pg C yr$^{-1}$ by the Northern Hemisphere ocean, and that this carbon is then transported southward by the ocean currents across the equator into the Southern Hemisphere, where it outgasses back into the atmosphere. Furthermore, they argued that this transport existed in preindustrial times and that it is balanced by a northward atmospheric transport of equal magnitude. Using an early, limited set of surface ocean observations of the partial pressure of CO$_2$ in the Northern Hemisphere oceans, *Tans et al.* [1990] rejected this hypothesis, and argued that the Northern Hemisphere sink was primarily due to the terrestrial biosphere. The debate about the nature of the Northern Hemisphere carbon sink has spawned a substantial number of investigations with conflicting conclusions [*Broecker and Peng*, 1992; *Keeling and Peng*, 1995; *Sarmiento et al.*, 2000].

[4] Separation of the natural from the anthropogenic CO$_2$ fluxes is also important to better understand the response of the ocean to climate change. Changes in ocean circulation, biology, and chemistry due to climate change act differently on the processes governing air-sea fluxes of anthropogenic and natural CO$_2$ because of the different timescales involved [*Sarmiento et al.*, 1998; *Joos et al.*, 1999; *Gruber et al.*, 2004]. While the total air-sea CO$_2$ flux can be estimated from observations of the difference between the partial pressure of CO$_2$ in the atmosphere and that in the

surface ocean, $\Delta$pCO$_2$, and a parametrization of the air-sea gas exchange coefficient [e.g., *Takahashi et al.*, 2002], the air-sea flux of natural CO$_2$ cannot be estimated using this method. In contrast, such a separation has been achieved for ocean interior data, permitting us to determine the footprint of natural air-sea gas exchange in the interior ocean from observations of dissolved inorganic carbon (*DIC*) and additional tracers [*Gruber and Sarmiento*, 2002]. Thus, if the patterns in the ocean interior data can be related to surface exchange by reversing the effect of mixing and advective transport in the oceans, we can, in principle, estimate the two flux components separately.

[5] To achieve this goal, an ocean inversion technique has recently been developed to estimate air-sea fluxes of heat and trace gases on the basis of ocean interior observations and OGCMs [*Gloor et al.*, 2001; *Gruber et al.*, 2001; *Gloor et al.*, 2003; *Mikaloff Fletcher et al.*, 2006; *Jacobson et al.*, 2007a, 2007b]. This approach is based on a Green's function inverse method that was adapted from atmospheric tracer inversions [e.g., *Enting and Mansbridge*, 1989; *Tans et al.*, 1990; *Bousquet et al.*, 2000]. The surface of the ocean is divided into discrete spatial regions, and an OGCM is used to simulate how an arbitrary flux into each region influences tracer concentrations in the interior ocean. Then we find the combination of fluxes from the prescribed regions that are in optimal agreement with the observations using a least squares technique.

[6] *Gloor et al.* [2003] presented the first ocean inversion estimates of the air-sea flux of CO$_2$ that resolved 13 ocean regions using three versions of an OGCM with varying subgridscale process parameterizations. A limited set of sensitivity studies suggested that the inverse estimates may be sensitive to biases in the OGCM used to represent transport and the method used to separate the anthropogenic and natural gas exchange components from the observed *DIC* [*Gloor et al.*, 2003]. *Mikaloff Fletcher et al.* [2006] revisited the anthropogenic carbon inversion employing a suite of 10 OGCMs to quantify the uncertainties associated with the representation of ocean transport and incorporating many additional improvements, such as a larger number of regions, better representation of the spatial distribution of the fluxes within these regions, and improved consideration of the uncertainty associated with the observations. They also examined the sensitivity of the anthropogenic CO$_2$ uptake results to biases in the data-based estimates of anthropogenic CO$_2$ in detail.

[7] Combining the oceanic with the atmospheric inversion, *Jacobson et al.* [2007a, 2007b] developed a joint atmosphere-ocean inversion method, which estimates the exchange of CO$_2$ between the atmosphere and all of the Earth's surface, i.e., both ocean and land regions. The spatial gradients of CO$_2$ fluxes in the Southern Hemisphere from the ocean inversion combined with spatial gradients in atmospheric CO$_2$ suggest that there must be a large source from the southern terrestrial land regions, which remained unresolvable in earlier atmospheric inversion studies primarily because these studies were not able to effectively partition the ocean sink from the land source in the tropics and Southern Hemisphere using atmospheric CO$_2$ observations alone.

[8] We expand on this body of work with an in-depth study of the air-sea fluxes of the natural CO$_2$ analogous to the anthropogenic carbon study of *Mikaloff Fletcher et al.* [2006]. A discussion of the contemporary CO$_2$ fluxes, i.e., the sum of the natural and anthropogenic fluxes, will be provided by N. Gruber et al. (Oceanic sources and sinks for atmospheric CO$_2$, submitted to *Global Biogeochemical Cycles*, 2007) (hereinafter referred to as Gruber et al., submitted manuscript, 2007). Here we present air-sea fluxes of natural CO$_2$ from 23 ocean regions estimated using a suite of 10 different OGCMs. This regional configuration gives substantially higher resolution than *Gloor et al.* [2003]. In particular, we distinguish between the Southern Ocean regions differently from the previous study, which helps clarify the flux dynamics in this key region of atmosphere-ocean carbon exchange. We discuss the natural transport of carbon in the interior ocean and explore the implications of this transport for the global carbon cycle and the interpretation of spatial gradients in atmospheric CO$_2$. We quantify the uncertainties associated with the fluxes using the different OGCMs and nine possible scenarios for biases in the estimated air-sea gas exchange component of *DIC*.

## 2.  Methods

[9] The ocean inversion method used here was developed by *Gloor et al.* [2003]. We expand upon this work by using a larger number of model regions, refining the method, and engaging in a detailed investigation of the sensitivity of the estimated fluxes of natural CO$_2$ to potential biases. We therefore provide a brief overview of the method only, focusing on the differences between this work and earlier studies.

### 2.1.  Observations

[10] We employ *DIC*, alkalinity (*Alk*), phosphate (PO$_4^{3-}$), and other hydrographic data from the Global Ocean Data Analysis Project [*Key et al.*, 2004], which synthesized data primarily from the World Ocean Circulation Experiment (WOCE) and the Joint Global Ocean Flux Study (JGOFS). We also included observations from the TTO-NAS, TTO-TTS, and SAVE historical cruises [*Gruber*, 1998], which are of comparable quality to the WOCE data [*Tanhua and Wallace*, 2005]. The resulting data set has over 68,000 observations with excellent spatial coverage (see Figure S1 of the auxiliary material[1]).

[11] One challenge associated with using these data to determine air-sea fluxes is that *DIC* is not conserved in the interior ocean, but is subject to intense transformations due to biological processes. We employ a quasiconservative tracer, $\Delta C_{gasex}$ [*Gruber and Sarmiento*, 2002], which is closely related to the quasiconservative tracer $\Sigma^*$ of *Broecker and Peng* [1992]. This tracer is modified at the surface by the exchange of CO$_2$ across the air-sea interface, but is conserved in the interior ocean. $\Delta C_{gasex}$ is based on the observation that biological processes influence ocean

interior *DIC*, phosphate (PO$_4^{3-}$), and alkalinity (*Alk*) concentrations with relatively constant stoichiometric ratios. Therefore one can remove the biological signal using the observed PO$_4^{3-}$, *Alk*, and stoichiometric ratios. The anthropogenic carbon concentration is removed using a data-based estimate of anthropogenic carbon, $C_{ant}$, estimated following the $\Delta C^*$ method of *Gruber et al.* [1996]. This gives

$$\Delta C_{gasex} = \frac{S_o}{S}\left(DIC - r_{C:P}\cdot \text{PO}_4^{3-} - 0.5\cdot\left(Alk + r_{N:P}\text{PO}_4^{3-}\right)\right) - C_{ant} - constant, \tag{1}$$

where the constant is arbitrarily chosen such that the mean surface $\Delta C_{gasex}$ is zero. The value of this constant has no implications for our inversion results, as the inversion only interprets spatial gradients in $\Delta C_{gasex}$. The ratios $r_{C:P}$ and $r_{N:P}$ are the stoichiometric carbon-to-phosphorus and nitrogen-to-phosphorus ratios, respectively, for which we adopt the values determined by *Anderson and Sarmiento* [1994]. The tracer $\Delta C_{gasex}$ is normalized to a constant reference salinity, $S_o$ (35), to account for the concentration or dilution effect as a result of evaporation and precipitation. If the assumptions about the constant stoichiometric ratios are correct and the $C_{ant}$ estimate is accurate, gradients in $\Delta C_{gasex}$ are only caused by the exchange of natural CO$_2$ across the air-sea interface and ocean interior transport and mixing. Thus, if ocean interior patterns are combined with knowledge about ocean transport and mixing, one can infer the direction and magnitude of the implied air-sea flux (Figure 1).

[12] Since $\Delta C_{gasex}$ is a derived quantity, we have to consider the impact of uncertainty in this tracer on the inverse estimates. In addition to random measurement errors of *DIC*, *Alk*, and PO$_4^{3-}$, two sources of potential bias exist in $\Delta C_{gasex}$: biases in the stoichiometric ratios, $r_{C:P}$ and $r_{N:P}$, and biases in the data-based $C_{ant}$ estimates. These sources of error will be discussed in depth and quantified in section 4.2.

### 2.2.  Inverse Method

[13] We use a Green's function approach to estimate regional fluxes of natural CO$_2$ from the data-based $\Delta C_{gasex}$ estimates [*Gloor et al.*, 2001; *Mikaloff Fletcher et al.*, 2006]. The surface of the ocean is first divided into a number of regions (Figure 2). An OGCM is then used to create a basis function for each region, which provides a spatial pattern of ocean interior concentrations that results from an arbitrary flux of a dye tracer into the surface of that region. These basis functions were generated by each of the 10 participating OGCMs following the protocol of *Mikaloff Fletcher et al.* [2003]. In order to estimate the fluxes at the surface, each $\Delta C_{gasex}$ estimate is treated as a linear combination of the source strengths multiplied by the basis functions plus a globally uniform constant, which we also estimate. Each member of the resulting set of linear equations is then divided by an uncertainty estimate, which determines its weighting. Finally, a singular value decomposition (SVD) [*Press et al.*, 1992] is used to solve for the combination of source strengths that best matches the observations.
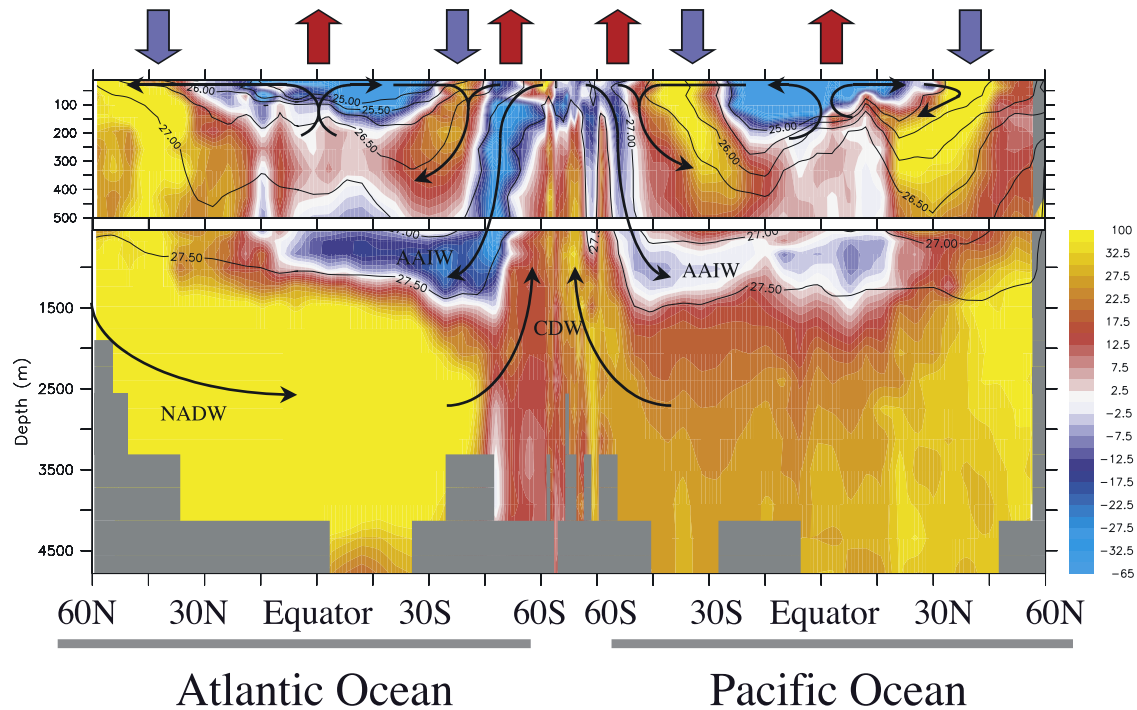
---

**Figure 1.** A global section of $\Delta C_{gasex}$ ($\mu$mol kg$^{-1}$) along a track that follows the global-scale deep-ocean circulations. This track begins in the Atlantic, just south of Iceland, and heads south to 60°S. It then turns east, and follows the 60°S latitude circle to 150°W, where it heads northward into the Pacific to 60°N. A few selected isopycnals are shown as contour lines, major flows are shown as narrow, black arrows, and air-sea fluxes are shown as thick, shaded arrows. The labels indicate locations of the following water masses: North Atlantic Deep Water (NADW), Antarctic Intermediate Water (AAIW), and Circumpolar Deep Water (CDW).

[14] The uncertainty used to weight each observational constraint is calculated by the propagation of random errors associated with $\Delta C_{gasex}$. The random errors associated with the stoichiometric ratios are taken from *Anderson and Sarmiento* [1994], the random errors associated with $C_{ant}$ are calculated following *Gruber et al.* [1996], and the measurement errors associated with the observations of *DIC*, PO$_4^{3-}$, and *Alk* are taken to be 2.0 $\mu$mol kg$^{-1}$, 0.05 $\mu$mol kg$^{-1}$, and 1.0 $\mu$mol kg$^{-1}$, respectively [*Wallace*, 2001]. Another type of error that is sometimes considered when weighting the data is representation error, which reflects how well point observations can be described by a coarse resolution model. Unfortunately, it is difficult to accurately assess the magnitude of this error. We add a spatially uniform uncertainty of 10 $\mu$mol kg$^{-1}$ to account for representation error, but we also tested a variety of different weighting schemes. The inverse air-sea flux estimates are insensitive to the choice of weighting scheme owing to the large number of observations and the strong spatial gradients in $\Delta C_{gasex}$.

[15] The inversely estimated partitioning between air-sea fluxes into a few regions is unstable owing to a high similarity between the spatial structure of the basis functions, data limitations, or both. However, the inversion is able to constrain the sum of these regional fluxes, so this problem can largely be avoided by combining regions. The inversion was done using the original 30 regions, and the results were then combined to the 23 regions reported here (Figure 2). We aggregated regions that had high off-diagonal elements of the matrix of region-region air-sea flux covariances, which is calculated as part of the SVD [*Press et al.*, 1992]. The diagonal elements of this matrix represent the square of the random error associated with each air-sea flux estimate, and the off-diagonal elements represent the covariances between regional flux estimates (Figure S3 of the auxiliary material). Large covariances between two or more regions indicate that the partitioning between these regions may be unstable. Even after aggregating to 23 regions, there remain substantial covariances between the air-sea fluxes in the South Sub-polar Atlantic, the South Sub-polar Indian and Pacific, and the Polar Southern Ocean (Figure 2). The longitudinal separation of the fluxes south of 44°S is therefore expected to be uncertain. However, the meridional partitioning of the fluxes between the regions south of 44°S and those north of this boundary is well constrained by the inversion.

### 2.3. Ocean Transport Models

[16] In order to account for biases due to model transport, the inverse calculations were done using basis functions generated by a suite of 10 OGCMs (Table S1 of the auxiliary material). Simulations were undertaken by six different modeling groups: Princeton (PRINCE),
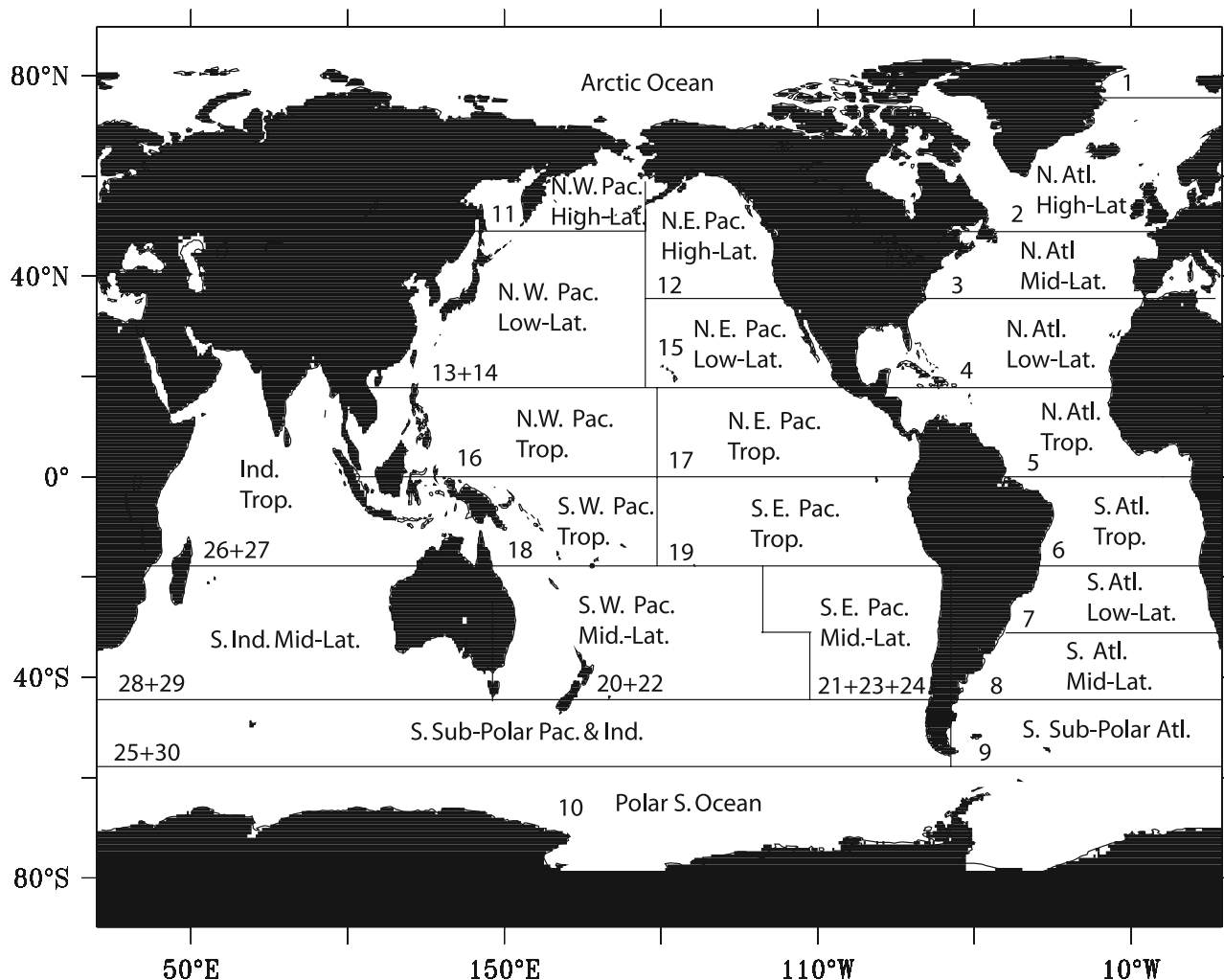
**Figure 2.** The 23 regions used for the ocean inversion. The region numbers show the aggregation from the original 30 regions [*Mikaloff Fletcher et al.*, 2003] to the 23 regions used in this study.

Massachusetts Institute of Technology (MIT), Bern-Switzerland (Bern3D), Jet Propulsion Laboratory (ECCO), National Center for Atmospheric Research (NCAR), and University of Liége-Belgium (UL). The individual models are described in further detail by *Mikaloff Fletcher et al.* [2006]. The Princeton group computed basis functions for five different configurations of their model [*Gnanadesikan et al.*, 2002, 2004], which have been shown to span the range of a larger group of OGCMs used in OCMIP-2 [*Matsumoto et al.*, 2004]. These five sets of PRINCE basis functions are the same ones that were used by *Jacobson et al.* [2007a, 2007b].

[17] Comparisons between the modeled and the observed distributions of CFCs, radiocarbon, and other tracers have shown that not all OGCMs represent transport and mixing with equal accuracy [e.g., *Doney et al.*, 2004; *Dutay et al.*, 2002; *Matsumoto et al.*, 2004; *Müller et al.*, 2006]. In order to address this, we employ a model skill score based on the formula of *Taylor* [2001], which is based on the correlation between the observed and modeled quantities and the ratio of the standard deviation of the model results to the standard deviation of the observations. Natural radiocarbon from the GLODAP data set [*Key et al.*, 2004] was used to calculate the skill score because it is a passive, approximately conservative tracer in the ocean interior, it has been widely measured, and it is transported on a similar timescale as natural carbon. The model simulations of natural radiocarbon were done following the OCMIP-2 protocol of *Orr et al.* [1999] for all of the models participating in this study except ECCO and MIT. The radiocarbon skill score was then used to weight the cross-model averages and standard deviations reported throughout the rest of this paper according to the formulas given in the supplementary materials of *Mikaloff Fletcher et al.* [2006]. Models without a skill score were not included in the weighted mean values.

## 3. Results and Discussion

### 3.1. Natural Air-Sea Fluxes of CO$_2$

#### 3.1.1. Inverse Estimates

[18] Globally, the ocean inversion finds a nearly balanced exchange, with a mean flux of $-0.03 \pm 0.08$ Pg C yr$^{-1}$ (see

**Table 1.** Inverse Air-Sea Flux of Natural Carbon Based on Basis Functions From 10 Different OGCMS[a]

| | Area, $10^{12}$ m$^2$ | Bern3D, Pg C yr$^{-1}$ | ECCO, Pg C yr$^{-1}$ | MIT, Pg C yr$^{-1}$ | NCAR, Pg C yr$^{-1}$ | PRINCE-LL, Pg C yr$^{-1}$ | PRINCE-HH, Pg C yr$^{-1}$ | PRINCE-LHS, Pg C yr$^{-1}$ | PRINCE-2, Pg C yr$^{-1}$ | PRINCE-2a, Pg C yr$^{-1}$ | UL, Pg C yr$^{-1}$ | Mean ± Std. Dev., Pg C yr$^{-1}$ |
|---|---|---|---|---|---|---|---|---|---|---|---|---|
| Arctic Ocean | 16.09 | 0.01 | −0.01 | 0.00 | −0.01 | −0.02 | −0.02 | −0.02 | −0.02 | −0.03 | −0.07 | −0.02 ± 0.02 |
| N. Atl. High-Lat. | 9.87 | −0.14 | −0.14 | −0.03 | −0.13 | −0.07 | −0.10 | −0.08 | −0.08 | −0.08 | −0.19 | −0.11 ± 0.04 |
| N. Atl. Mid-Lat. | 9.90 | −0.09 | −0.17 | −0.22 | −0.20 | −0.11 | −0.13 | −0.12 | −0.12 | −0.13 | −0.08 | −0.12 ± 0.04 |
| N. Atl. Low-Lat. | 14.73 | −0.09 | −0.04 | −0.04 | −0.01 | −0.11 | −0.10 | −0.11 | −0.11 | −0.09 | −0.01 | −0.08 ± 0.04 |
| N. Atl. Trop. | 12.61 | 0.03 | −0.01 | 0.05 | 0.01 | 0.03 | 0.05 | 0.03 | 0.03 | 0.03 | 0.02 | 0.03 ± 0.01 |
| S. Atl. Trop. | 10.55 | 0.10 | 0.11 | 0.12 | 0.12 | 0.15 | 0.16 | 0.15 | 0.15 | 0.15 | 0.11 | 0.14 ± 0.02 |
| S. Atl. Low-Lat. | 9.02 | 0.01 | 0.02 | 0.01 | 0.02 | 0.02 | −0.01 | 0.02 | 0.02 | 0.03 | 0.03 | 0.02 ± 0.01 |
| S. Atl. Mid-Lat. | 9.48 | −0.05 | −0.10 | −0.11 | −0.06 | −0.15 | −0.14 | −0.15 | −0.16 | −0.14 | −0.05 | −0.11 ± 0.05 |
| S. Sub-Polar. At. | 8.81 | 0.03 | 0.10 | 0.05 | 0.10 | 0.10 | 0.14 | 0.14 | 0.15 | 0.18 | 0.08 | 0.11 ± 0.05 |
| Polar S. Ocean | 28.88 | 0.06 | 0.13 | −0.05 | 0.01 | 0.09 | −0.03 | 0.07 | 0.02 | 0.02 | 0.08 | 0.04 ± 0.04 |
| N.W. Pac. High-Lat | 4.19 | 0.03 | 0.04 | 0.03 | 0.09 | 0.02 | 0.05 | 0.02 | 0.03 | 0.03 | 0.02 | 0.04 ± 0.02 |
| N.E. Pac. High-Lat. | 7.22 | −0.04 | −0.03 | −0.11 | 0.04 | −0.03 | −0.03 | −0.03 | −0.03 | −0.03 | −0.01 | −0.02 ± 0.03 |
| N.W. Pac. Low-Lat. | 22.22 | −0.19 | −0.29 | −0.22 | −0.32 | −0.27 | −0.36 | −0.27 | −0.30 | −0.30 | −0.28 | −0.29 ± 0.05 |
| N.E. Pac. Low-Lat. | 10.61 | −0.01 | −0.01 | −0.04 | −0.02 | −0.02 | −0.03 | −0.02 | −0.02 | −0.02 | −0.02 | −0.02 ± 0.01 |
| N.W. Pac. Trop. | 19.61 | 0.09 | 0.01 | 0.07 | 0.00 | 0.06 | 0.12 | 0.06 | 0.07 | 0.05 | 0.08 | 0.07 ± 0.04 |
| N.E. Pac. Trop. | 16.77 | 0.09 | 0.14 | 0.21 | 0.15 | 0.12 | 0.20 | 0.12 | 0.16 | 0.22 | 0.14 | 0.15 ± 0.04 |
| S.W. Pac. Trop. | 12.07 | 0.04 | 0.02 | 0.06 | 0.06 | 0.02 | 0.08 | 0.02 | 0.04 | 0.03 | 0.05 | 0.05 ± 0.02 |
| S.E. Pac. Trop. | 18.35 | 0.40 | 0.30 | 0.24 | 0.23 | 0.42 | 0.43 | 0.42 | 0.41 | 0.24 | 0.34 | 0.36 ± 0.08 |
| S.W. Pac. Mid-Lat. | 24.82 | −0.45 | −0.29 | −0.32 | −0.26 | −0.34 | −0.49 | −0.33 | −0.34 | −0.36 | −0.21 | −0.35 ± 0.09 |
| S.E. Pac. Mid-Lat. | 13.83 | −0.02 | 0.05 | 0.06 | 0.03 | −0.02 | 0.00 | −0.03 | −0.04 | 0.03 | 0.00 | −0.01 ± 0.03 |
| S. Sub-Pol. Pac. + Ind | 28.65 | 0.23 | 0.24 | 0.33 | 0.12 | 0.24 | 0.28 | 0.27 | 0.30 | 0.42 | 0.17 | 0.25 ± 0.09 |
| Trop. Ind. | 32.27 | 0.11 | 0.10 | 0.13 | 0.13 | 0.14 | 0.18 | 0.14 | 0.15 | 0.12 | 0.15 | 0.14 ± 0.02 |
| S. Ind. Mid-Lat. | 26.30 | −0.11 | −0.25 | −0.31 | −0.24 | −0.26 | −0.17 | −0.26 | −0.26 | −0.28 | −0.24 | −0.22 ± 0.06 |
| Global total | | 0.05 | −0.08 | −0.10 | −0.14 | 0.01 | 0.05 | 0.03 | 0.05 | 0.08 | 0.10 | 0.03 ± 0.08 |
| Model skill score | | 0.93 | NA | NA | 0.94 | 0.65 | 0.97 | 0.76 | 0.92 | 0.91 | 0.86 | |
| Mean of the residuals[b] | | −2.9 | −3.5 | −3.6 | −2.0 | −3.5 | −2.7 | −3.1 | −2.9 | −2.5 | −1.2 | |

[a]Positive values indicate flux out of the ocean. Region boundaries are shown in Figure 2.
[b]Defined as the observed $\Delta C_{gasex}$ minus the $\Delta C_{gasex}$ reconstructed using the inverse estimates in units of $\mu$mol kg$^{-1}$.
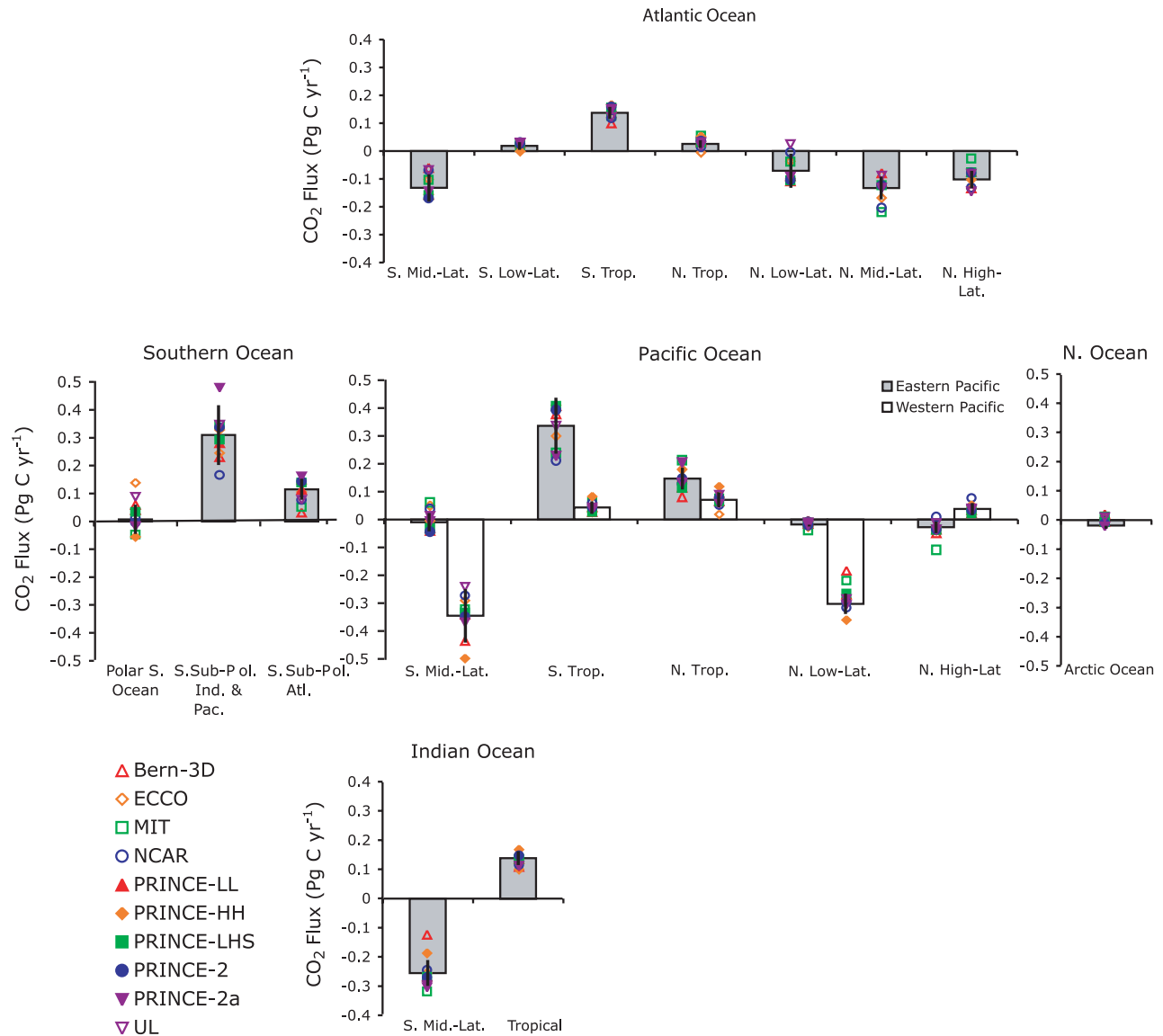
**Figure 3.** Inverse estimates the air-sea flux of natural $CO_2$ (Pg C $yr^{-1}$). Positive (negative) values indicate outgassing (uptake) by the ocean. The columns show the cross-model means and the error bars represent the standard deviation, both weighted by the model's radiocarbon skill scores (see Table S1 of the auxiliary material). The flux estimates for individual models are shown as symbols.

Table 1; here and throughout the rest of the paper "flux" refers to air-sea flux and transport refers to ocean interior transport.) This nearly balanced global flux estimate emerges naturally from our inversion, as we did not impose any constraints on the global integral flux. The finding of a near-zero flux is notable, because, in steady state, riverine carbon inputs are expected to lead to an outgassing of natural $CO_2$ of about 0.6 Pg C $yr^{-1}$ [*Sarmiento and Sundquist*, 1992].

[19] There are two possible scenarios for the influence of riverine carbon on the ocean inversion. The bulk of the organic and inorganic carbon from rivers might be buried in sediments or emitted to the atmosphere in coastal areas,

estuaries, tidal flats, rivers, or other areas not observed, and therefore would not be captured by the data set used to constrain the inversion owing to spatial sampling that avoids these areas. If this is the case, the open ocean air-sea flux estimates presented here are essentially independent of riverine carbon.

[20] A second possibility is that riverine carbon reaches the open ocean and is subsequently outgassed to the atmosphere. Riverine carbon would then increase the $\Delta C_{gasex}$ tracer concentrations because riverine discharge has a far greater carbon-to-phosphorus ratio in both organic and inorganic phases than the open ocean [*Lerman et al.*, 2004], which would lead to an apparent oceanic carbon

uptake in the inversion. In contrast, the loss of river derived $CO_2$ by outgassing is correctly diagnosed from the inversion from the corresponding decrease in $\Delta C_{gasex}$. Therefore, if riverine carbon is outgassing in the same model region where it enters the ocean, we expect essentially no effect of riverine carbon on the ocean inversion. If the riverine carbon is transported to other regions before being out-gassed, the inverse flux results are biased toward an uptake from the atmosphere by the amount of riverine carbon that escapes burial. Owing to our assumption of steady state, this bias is equal to the riverine outgassing of natural $CO_2$, explaining the nearly balanced global flux emerging from the inversion, despite the presence of a net river carbon driven outgassing of natural $CO_2$. Globally, *Jacobson et al.* [2007a] estimated this riverine outgassing outside of near-shore regions to about 0.45 Pg C yr$^{-1}$. When the inverse estimates of the fluxes of natural and anthropogenic $CO_2$ are combined to estimate the contemporary flux in order to compare, for example, to $\Delta pCO_2$ based estimates (Gruber et al., submitted manuscript, 2007) or to combine them with atmospheric constraints [*Jacobson et al.*, 2007a, 2007b], one needs to add an estimate of this riverine carbon flux to the inverse estimates. However, we decided here not to include these small corrections, as they are rather uncertain, and since we do not make comparisons that would require their consideration.

[21] Spatially, the ocean inversion finds uptake of natural $CO_2$ at midlatitudes in both hemispheres as well as in the Northern Hemisphere high latitudes, and outgassing in the tropics and in the Southern Ocean (Figure 3 and Table 1). This pattern is driven by spatial patterns in the observed $\Delta C_{gasex}$ (Figure 1). Relatively high values of this tracer indicate that when the water mass was last at the surface, it took up $CO_2$ from the atmosphere and relatively low values indicate that it has lost $CO_2$ to the atmosphere. For example, waters that upwell into the Tropical Pacific tend to have $\Delta C_{gasex}$ concentrations of around 0 $\mu$mol kg$^{-1}$, while subtropical surface waters in the Pacific tend to have $\Delta C_{gasex}$ concentrations of around 40 $\mu$mol kg$^{-1}$ or less. This implies that waters have lost over 40 $\mu$mol kg$^{-1}$ of natural $CO_2$ to the atmosphere between the point of upwelling and their poleward transport in the subtropics. If we neglect mixing, this can be interpreted as the signature of the Tropical Pacific $CO_2$ source.

[22] All of the models find substantial outgassing between 44°S and 59°S, with a mean of 0.37 ± 0.13 Pg C yr$^{-1}$ (Figure 3). This outgassing can be interpreted using $\Delta C_{gasex}$, which shows high values in the waters that upwell to the surface in this region, but has much lower values in the waters downstream, particularly in Sub-Antarctic Mode Water (SAMW) (Figure 1). The $\Delta C_{gasex}$ concentration difference is about −60 $\mu$mol kg$^{-1}$, which, when multiplied by an estimate of the mean overturning transport in the upper 100 m of about 10 to 20 Sv between 44°S and 59°S, gives a rough estimate of 0.4 Pg C yr$^{-1}$ outgassing, consistent with the inverse estimate.

[23] This outgassing is likely driven by the upwelling of waters with high concentrations of remineralized *DIC*, a substantial fraction of which can escape into the atmo-sphere as the carbon uptake by biology at the surface in the

Southern Ocean is slow and inefficient [*Gruber and Sarmiento*, 2002; *Murnane et al.*, 1999]. The inefficient biological pump in the Southern Ocean is thought to be the result of a combination of light limitation, iron limitation, and to a lesser extent, grazing. There is little net air-sea heat flux south of 50°S [*da Silva et al.*, 1994; *Gloor et al.*, 2001], so any solubility-driven $CO_2$ flux is small.

[24] In the midlatitudes of the Southern Hemisphere (18°S to 44°S), the ocean inversion estimates a vigorous uptake of natural $CO_2$ with a mean of 0.68 ± 0.13 Pg C yr$^{-1}$ (Figure 3). In the surface waters of the Southern Hemi-sphere midlatitudes, $\Delta C_{gasex}$ is relatively low, −35 to −60 $\mu$mol kg$^{-1}$ (Figure 1), but the $\Delta C_{gasex}$ concentra-tions increase substantially to the south of this, reflecting the uptake of $CO_2$ from the atmosphere. This uptake is likely driven by a combination of an efficient biological pump, and cooling of surface waters that are transported southward by Ekman circulation [*Murnane et al.*, 1999; *Gruber and Sarmiento*, 2002].

[25] The inversion estimates 0.93 ± 0.16 Pg C yr$^{-1}$ of outgassing in the tropics (18°N to 18°S) with approximately two thirds of this occurring in the Pacific Ocean (Figure 3). The signal of equatorial outgassing can be identified in the $\Delta C_{gasex}$ distribution, as the upper thermocline waters that upwell in the tropics have high concentrations of $\Delta C_{gasex}$, while the $\Delta C_{gasex}$ values of the near-surface waters that are transported poleward by Ekman transport are much lower. The outgassing in the tropics results from upwelling of waters that are rich in remineralized *DIC*, which the biological pump is unable to fix before it escapes to the atmosphere. The upwelled waters undergo substantial warming, resulting in a substantial solubility pump contri-bution to the total outgassing [*Murnane et al.*, 1999; *Gruber and Sarmiento*, 2002].

[26] In the mid and high latitudes of the Northern Hemi-sphere, the ocean inversion finds uptake of natural $CO_2$ nearly everywhere, with the highest uptake fluxes occurring in the North Atlantic (Figure 3). This is consistent with the high concentrations of $\Delta C_{gasex}$ observed in the deep Atlan-tic (Figure 1), which imply a substantial uptake of $CO_2$ from the atmosphere.

[27] As discussed by *Broecker and Peng* [1992], the high $CO_2$ uptake in the North Atlantic is the result of a combi-nation of cooling of warm waters of subtropical origin as they move poleward and a highly efficient biological carbon pump [see also *Gruber and Sarmiento*, 2002]. The $CO_2$ uptake is significantly smaller in the North Pacific, primar-ily because the biological pump is substantially less efficient there, but also because there is somewhat less cooling, and no deep water formation in this basin.

### 3.1.2. Comparison With Forward Simulations

[28] The inversely estimated air-sea fluxes of natural $CO_2$ are generally similar to many of those derived from simu-lations, in which an OGCM is combined with a biogeo-chemistry model and integrated forward in time to equilibrium [e.g., *Murnane et al.*, 1999; *Sarmiento et al.*, 2000; *Watson and Orr*, 2003; *Wetzel et al.*, 2005], but differ substantially in a number of critical aspects. We first compare our results with the OCMIP-2 results, which use a simple ecosystem/biogeochemistry model [*Najjar and*
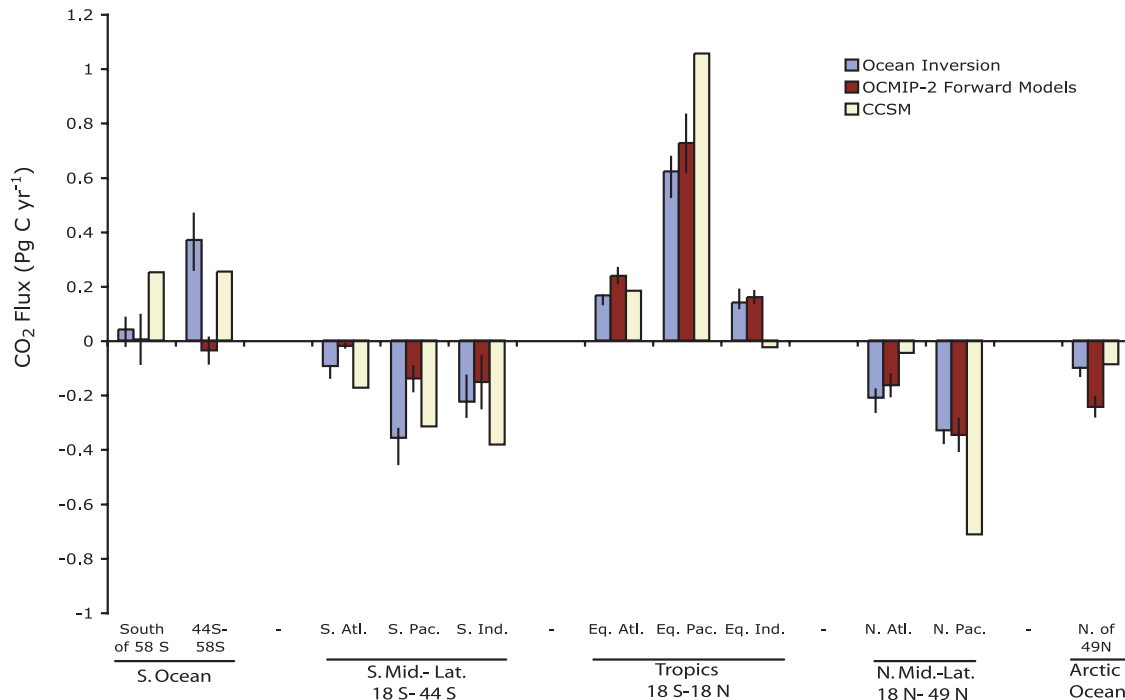
**Figure 4.** Comparison between flux estimates of natural $CO_2$ from the ocean inversion, forward simulations from OCMIP-2, and forward simulations from the CCSM coupled with the ecosystem and biogeochemistry model described by *Moore et al.* [2004]. The OCMIP-2 results only include those models that participated in both the ocean inversion and OCMIP-2 (NCAR, PRINCE (NCAR, PRINCE-LL, PRINCE-HH, PRINCE-LHS, PRINCE-2, PRINCE-2a, and UL), and the mean and standard deviation have been weighted using the same radiocarbon skill score weighting as the ocean inversion. The shaded bars represent the radiocarbon skill score weighted cross-model means and the error bars represent the weighted standard deviation between models. The fluxes have been aggregated to 11 regions for clarity. Positive (negative) values indicate outgassing (uptake).

*Orr*, 1999] (also R. G. Najjar et al., Impact of circulation on export production, dissolved organic matter and dissolved oxygen in the ocean: Results from OCMIP-2, submitted to *Global Biogeochemical Cycles*, 2007) (hereinafter referred to as Najjar et al., submitted manuscript, 2007). We used only those OCMIP-2 models that participated in both OCMIP-2 and this study, permitting us to largely remove differences due to model transport alone, and weighted them using the radiocarbon skill score in exactly the same way. Afterward, we compare the inverse estimates with a wider range of forward simulations.

[29] Figure 4 reveals that the OCMIP-2 forward and inverse estimates generally agree to within the error bars in the tropics and in the midlatitudes of the Northern Hemisphere (see also Table S2 of the auxiliary material). However, there are substantial differences in the Southern Hemisphere, particularly between 18°S and 44°S, where the OCMIP-2 forward simulations find less than half as much natural $CO_2$ uptake as the inversion. In addition, the forward simulations simulate very little flux south of 44°S 0.37 ± 0.13 Pg C yr$^{-1}$.

[30] This spatial pattern of relatively little air-sea flux of natural $CO_2$ south of 18°S in the OCMIP-2 simulations is qualitatively comparable to a number of previous forward simulations [e.g., *Murnane et al.*, 1999; *Sarmiento et al.*, 2000; *Wetzel et al.*, 2005]. However, some more recent forward simulations using more complex biological models and different physics are in far better agreement with the inverse estimates in the Southern Hemisphere [*Moore et al.*, 2004; *Doney et al.*, 2006]. For example, fluxes of natural $CO_2$ from the ocean component of the Community Climate System Model (CCSM) coupled with the ecosystem and biogeochemistry model described by *Moore et al.* [2004] are within the error bars associated with the inverse estimates between 18°S and 44°S (Figure 4). The inversion still finds about twice as much $CO_2$ outgassing as the CCSM forward simulation south of 44°S, largely owing to the inversion estimating substantial outgassing in the South Sub-polar Atlantic while the CCSM forward simulation finds a small net uptake.

[31] The differences in the Southern Hemisphere between the ocean inversion and OCMIP-2 as well as many other previous forward modeling studies could be due to biases in the inversion, discussed in section 4. However, all of the scenarios constructed to test potential sources of error robustly find this meridional source and sink pattern. Alternatively, the differences between the OCMIP-2 forward and the inverse flux estimates could be due to errors in

the biogeochemical model used in the OCMIP-2 forward simulations. For example, the spatial and seasonal structure of the nutrient restoring fields is not well known, and seasonal phase lags in the nutrient restoring fields may cause considerable biases (Najjar et al., 2007). In addition, the OCMIP-2 forward simulations are sensitive to the parameterization of organic matter cycling, the lifetime of *DOC*, and remineralization length scales of sinking particulate matter. The small net natural CO$_2$ fluxes exhibited by the OCMIP-2 models south of 18°S are the result of a near-cancellation of a strong uptake flux due to the solubility pump and a nearly equally strong outgassing flux due to the biological pump [*Murnane et al.*, 1999; *Sarmiento et al.*, 2000; *Watson and Orr*, 2003]. Therefore it is conceivable that a slight imbalance in these two pumps or meridional shifts in the location of the maximum influence of the two pumps is all that is needed in order for the forward simulations to reproduce the pattern identified by the inversion. The new forward results of the CCSM tend to support this conclusion.

### 3.1.3. Comparison With Previous Inverse Estimates

[32] This work is generally in good agreement with the previous ocean inversion study of *Gloor et al.* [2003], except that they did not identify the large gradients in the Southern Hemisphere flux pattern discussed above. This is primarily because a smaller number of regions was used, and the region selection happened to combine part of the Southern Hemisphere midlatitude uptake region (north of 44°S to 18°S) with the Southern Hemisphere high-latitude outgassing region (south of 44°S), leading to a smooth pattern. When we interpolate our inverse flux estimates to the model regions of *Gloor et al.* [2003], our results are similar (Figure S2 of the auxiliary material).

[33] Other differences are *Gloor et al.* [2003] finding a higher uptake in the midlatitude South Pacific and midlatitude North Pacific, and stronger outgassing in the tropical Pacific (Figure S2 of the auxiliary material). This is likely also a consequence of their using a smaller number of model regions. The use of overly large model regions can lead to aggregation error because of the assumption that fluxes within these regions are proportional to a prescribed spatial pattern [*Kaminski et al.*, 2001]. Therefore our results are expected to be less biased. Another cause for the differences is that we report the mean from 10 OGCMs, while *Gloor et al.* [2003] report results primarily based on one model, PRINCE-LL, which is included in this study. Comparisons between *Gloor et al.* [2003] and the results from this work using only PRINCE-LL indicate that the OGCMs used has a smaller effect on the differences between flux estimates than the region selection. Additional, smaller methodological differences [*Mikaloff Fletcher et al.*, 2006] have little or no effect on the results.

[34] The flux estimates presented here are essentially identical to the natural CO$_2$ flux component of the joint atmosphere-ocean inversion of *Jacobson et al.* [2007b], except that we use a suite of 10 OGCMs, while *Jacobson et al.* [2007b] use only the five configurations of the PRINCE model, also included in this study. Differences between regional flux estimates for these two studies due to factors other than the OGCMs, for example, the use

of atmospheric data of *Jacobson et al.* [2007a], slightly different error weighting structures, and different minimization techniques, are generally less than 0.02 Pg C yr$^{-1}$ regionally.

### 3.2. Oceanic Transport of Natural CO$_2$

[35] The meridional transports implied by the inverse estimates are calculated by integrating the regional fluxes spatially, starting at the North Pole. Separation of the transports by individual basins requires the specification of the natural CO$_2$ transport by the Indonesian throughflow and the Bering Strait. These were computed for each model by multiplying the volume flux in the model for each vertical grid cell with the observed $\Delta C_{gasex}$ concentration interpolated to the throughflow point in the model. The observed $\Delta C_{gasex}$ concentrations at many depth levels are negative in these two regions; therefore, the direction of $\Delta C_{gasex}$ flow is opposite the direction of mass flux in the models. This can be physically interpreted as a southward (northward) transport of waters through the Indonesian Throughflow (Bering Strait) that have been depleted in carbon by outgassing to the atmosphere.

[36] We find substantial southward transport of natural CO$_2$ throughout the Atlantic Ocean (Figure 5). This is primarily the result of the uptake of natural CO$_2$ in the North Atlantic, which is then entrained into North Atlantic Deep Water (NADW) and transported southward in the deep ocean to the Southern Ocean, where it is eventually upwelled [*Broecker and Peng*, 1992]. In addition, the distribution of $\Delta C_{gasex}$ suggests that waters upwelled in the tropics release CO$_2$ to the atmosphere, then take up natural CO$_2$ as they move poleward. These waters are then subducted in the subtropical gyres and return $\Delta C_{gasex}$-rich water to the tropics (Figure 1).

[37] In the Pacific and Indian Oceans, the inverse flux estimates imply equatorward transport from midlatitudes and convergence in the tropics (Figure 5), due to the subduction and equatorward transport of $\Delta C_{gasex}$-rich waters in the subtropical gyres. The ocean inversion also finds substantial poleward transport across 44°S. This indicates that some of the natural CO$_2$ taken up at midlatitudes continues poleward.

[38] Analysis of the observed spatial gradients of atmospheric CO$_2$ indicate that there is at present (1980s and 1990s) a major sink of atmospheric CO$_2$ in the Northern Hemisphere [e.g., *Keeling et al.*, 1989a; *Tans et al.*, 1990]. However, there has been considerable debate about the nature of this sink, as discussed in section 1. *Keeling et al.* [1989b] proposed that the Northern Hemisphere carbon sink could be explained by a natural cycle of ∼1 Pg C yr$^{-1}$ southward oceanic transport balanced by an equal northward CO$_2$ transport in the atmosphere.

[39] We find a substantially smaller southward cross-equatorial transport of 0.31 ± 0.02 Pg C yr$^{-1}$, which primarily occurs in the Atlantic Ocean. The uncertainty estimate is based on the standard deviation between the models, which is taken after the cross-equatorial transports for the Atlantic, Pacific, and Indian Oceans are summed. Our small cross-equatorial transport estimate supports the hypothesis that there must be a substantial terrestrial carbon
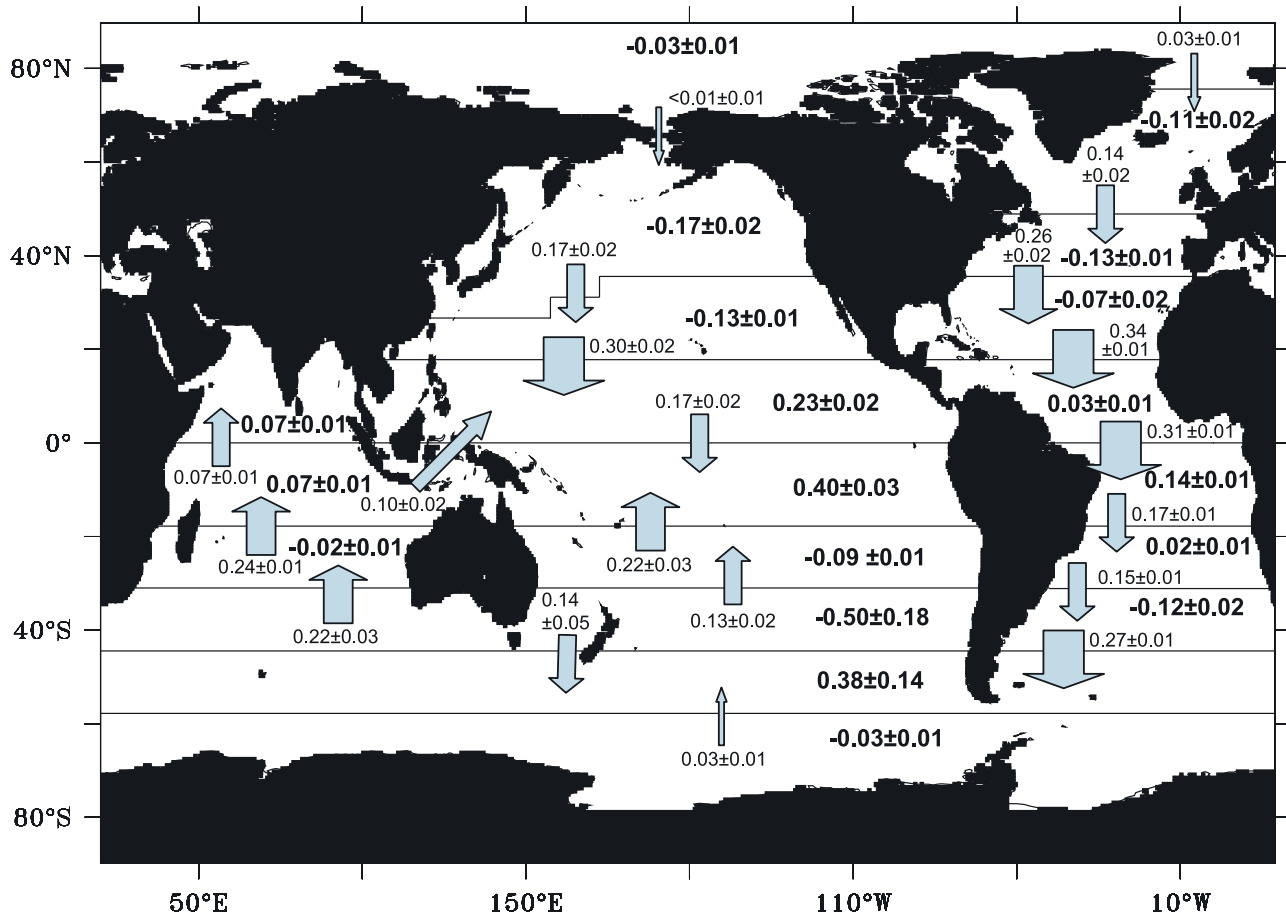
**Figure 5.** Global map of the transport (shown above or below arrows) of natural $CO_2$ (Pg C yr$^{-1}$) based on the inverse flux estimates (bold). The values shown are the weighted mean estimates and their weighted standard deviation. The transport estimates include only that component of *DIC* that reflects exchange with the atmosphere. The width of the arrows are only qualitatively proportional to the transports.

sink in the Northern Hemisphere [*Tans et al.*, 1990]. Nevertheless, our inversion gives a larger interhemispheric ocean carbon transport than the three forward simulations used in the OGCM study of *Sarmiento et al.* [2000], which found a slight southward cross-equatorial transport of 0.12 Pg C yr$^{-1}$. These differences are because the forward models used by *Sarmiento et al.* [2000] simulated less natural carbon uptake at northern high and mid latitudes and did not find substantial outgassing in the Southern Ocean.

[40] Natural $CO_2$ transport has also been estimated across several transects in the Atlantic Ocean on the basis of hydrographic data, using assumptions about the geostrophic nature of the flow, estimates of the Ekman-driven flow, and data-based estimates of natural carbon [e.g., *Brewer et al.*, 1989; *Lundberg and Haugan*, 1996; *Holfort et al.*, 1998; *Álvarez et al.*, 2003; *Rosón et al.*, 2003; *Macdonald et al.*, 2003]. Comparisons between inverse transport estimates and estimates based on hydrographic data need to be interpreted with care. The hydrographic data-based estimates determine the transport for a single point in time

and could be influenced by substantial seasonal or interannual variations in transport. By contrast, the inverse estimates reflect long-term mean transport. Because of the general lack of organic carbon measurements, the hydrographic data-based estimates also have to neglect the possible transport divergence that results from the transport divergence of organic carbon, but this is relatively small. The hydrographic data also include transport of riverine carbon, which may not be detected in the inversion as discussed in the following section. Finally, the hydrographic data-based estimates reflect the transport of the total *DIC* pool, i.e., also the nondivergent part due to net mass transport across a section. Our transport estimates reflect only the transport of the *DIC* pool that is divergent as a result of air-sea gas exchange. Therefore we subtract the estimated Bering Strait Throughflow reported in these studies (0.62–0.65 Pg C yr$^{-1}$) from the hydrographic data-based estimates, where applicable, so that all of the transport estimates are directly comparable.

[41] South of 20°S in the Atlantic, the estimated natural $CO_2$ transports generally agree to within the error estimates
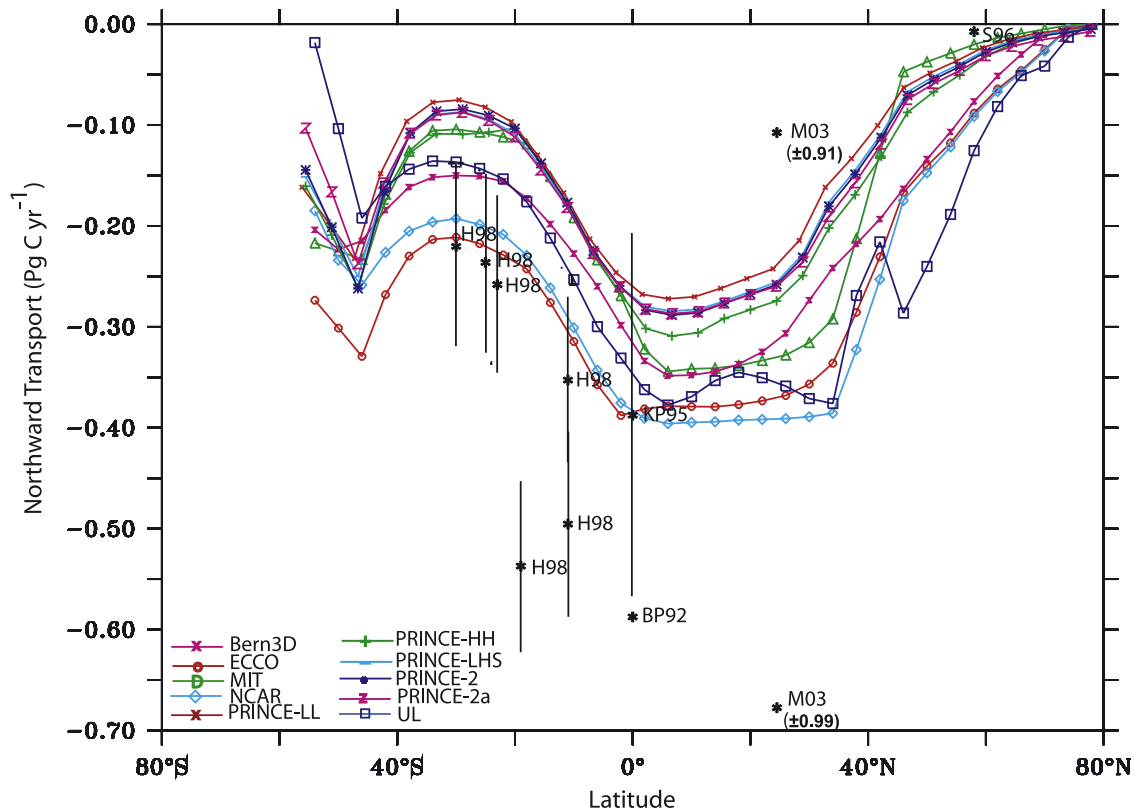
**Figure 6.** Inverse estimates of oceanic transport of natural CO$_2$ in the Atlantic Ocean (Pg C yr$^{-1}$) from the 10 participating OGCMS compared with estimates based on hydrographic transects. Shown are: *Holfort et al.* [1998] (H98), *Keeling and Peng* [1995] (KP95), *Broecker and Peng* [1992] (BP92), *Macdonald et al.* [2003] (M03), and *Stoll et al.* [1996] (S96). Separate transport values at the same latitude (H98 and M03) reflect analysis of data from separate cruises along the same transect. We subtracted the Bering Strait throughflow from H98, M03, and S96, so that they are comparable to the inverse estimates, as discussed in section 3.2. Negative values indicate southward transport.

between the two methods (Figure 6). However, the hydrographic data-based studies find substantially more southward transport of natural CO$_2$ in the midlatitude north and tropical Atlantic than the inverse estimates. We currently do not know the cause for these large differences. They may be partially due to seasonal or interannual biases in the hydrographic data-based estimates, or other sources of error discussed above. For example, the hydrographic data-based estimates across 24.5°N range from 0.12 to 0.69 Pg C yr$^{-1}$ of southward transport (after removing a 0.62 Pg C yr$^{-1}$ Bering Straight Throughflow) for different cruise years [*Macdonald et al.*, 2003]. Methodological errors in the hydrographic transect data may also be important. For example, *Rosón et al.* [2003] (not shown) estimate 0.46 Pg C yr$^{-1}$ greater transport across 24.5°N than *Macdonald et al.* [2003] using the same oceanographic data set. The discrepancy between natural carbon transport estimates in the North Atlantic may also be due to errors in the inversion. Nearly all coarse-resolution OGCMs form NADW that is too warm and too shallow. In the inversion, this may cause insufficient uptake of CO$_2$ from the atmosphere in the North Atlantic, and hence an underestimate of the southward transport.

## 4. Sensitivity and Error Analysis

[42] We test the sensitivity of the inversion to biases in $\Delta C_{gasex}$ and to biases stemming from errors in model transport. To this end, we employ a suite of 10 OGCMs and nine scenarios describing potential biases in $\Delta C_{gasex}$. However, there are a number of other sources of uncertainty that will not be quantified in this paper, which we discuss briefly here.

[43] One potentially important source of error is the implicit assumption that ocean circulation is approximately constant in time. The OGCMs used in this study have steady state circulation. Therefore any spatially coherent pattern in the observations that arises owing to variability in ocean circulation will cause shifts in the inversely estimated air-sea fluxes. Repeat hydrographic studies have found substantial evidence for decadal variability in ocean circulation [e.g., *Doney et al.*, 1998; *García et al.*, 2002; *Bryden et al.*, 2003; *Johnson and Gruber*, 2007; *McPhaden and Zhang*, 2002]. We are currently unable to quantify the

potential impact of biases owing to temporal variability in ocean circulation. Qualitatively, our method is most sensitive to long-term trends in ocean transport, resulting from, for example, the transition out of the little ice age or human induced climate change. Although a clear long-term warming trend of the ocean has been documented [*Levitus et al.*, 2000], the impact of this warming on ocean transport is currently believed to be relatively small. This is indicated, for example, by comparisons between observed and OGCM-simulated CFCs that do not indicate major problems in the model circulation due to temporal variability [*Dutay et al.*, 2002].

[44] Although we use a wide range of OGCMs to determine the sensitivity of the ocean inversion to transport, this does not address the possibility of fundamental errors that are common to all of the models, for example, the coarse resolution of all of the models, and the limited consideration of processes that lead to deep water formation. The coarse resolution of the models is of particular concern, since it precludes the models from explicitly resolving eddies and reproducing some major current systems.

[45] Another potential source of error is seasonal bias in the observations, particularly in the Southern Ocean. Observations of temperature, salinity, and other quantities have been used to restore or tune many of the OGCMs used in this study. There may also be some seasonal bias in the $\Delta C_{gasex}$ observations, but these biases are likely to be minimal in waters deeper than 200 m. Eighty percent of the observations in the ocean inversion are from waters deeper than 200 m.

[46] There may also be errors due to the inverse methodology. For example, the use of large spatial regions in inverse models can lead to aggregation errors due to the implicit assumption that fluxes over these regions are proportional to a prescribed spatial pattern that describes subregional variations in the fluxes [*Kaminski et al.*, 2001]. Nevertheless, on the basis of analysis of the covariance matrix discussed in section 2.2, we conclude that increasing the number of model regions further may lead to solutions that are not well constrained by the observations. We would therefore be required to either aggregate the regions to a similar configuration to the one used here or rely heavily on regularization techniques such as the imposition of a priori flux estimates or spatial correlations between regions.

[47] Finally, errors may arise owing to covariances between model regions that are difficult for the inversion to distinguish because their basis functions are too similar, they are not well sampled by the data, or both. The regional flux estimates corresponding to the original 30 regions have already been aggregated to 23 regions to eliminate the strongest covariances.

## 4.1. Sensitivity to Modeled Transport

[48] The principal features of the natural carbon fluxes and transports are remarkably insensitive to the choice of OGCM (Figures S4 and S5 of the auxiliary material). The cross-model standard deviation of the regional flux estimates are less than 33% of the total flux except in regions where both the flux and the uncertainty are small.

[49] The largest cross-model uncertainties in the inverse estimates occur in the temperate and high-latitude Southern Hemisphere, particularly in the Indian and Pacific. Previous model comparison studies such as OCMIP-2 have found substantial differences between OGCMs in the Southern Ocean [*Dutay et al.*, 2002; *Doney et al.*, 2004; *Mikaloff Fletcher et al.*, 2006]. The high cross-model differences in the Southern Hemisphere are partially due to the difficulty of correctly representing along-isopycnal transport, brine rejection due to sea ice formation, ice shelf processes, uncertainties in surface boundary conditions, the role of eddies and the way that they are parameterized, and the lack of data available to evaluate the models in this region [*Doney et al.*, 2004; *Caldeira and Duffy*, 2000].

[50] The cross-model standard deviation of the inverse flux estimates is always substantially greater than the random errors calculated from the diagonal elements of the covariance matrix, which reflect the uncertainty due to the ability of the observations to constrain the regional flux estimates and the random estimates for $\Delta C_{gasex}$. This supports the earlier conclusion that the ocean inversion is not limited by insufficient observational coverage [*Gloor et al.*, 2001, 2003].

[51] A three-dimensional distribution of the $\Delta C_{gasex}$ can be reconstructed by multiplying each basis function by the inverse flux estimate for that region and summing over all of the model regions. Residuals between the observed $\Delta C_{gasex}$ and reconstructed $\Delta C_{gasex}$ concentrations from the ocean inversion are a useful diagnostic for the inversion, since they highlight places where the basis functions are unable to reproduce the observations owing to errors in the models, errors in the $\Delta C_{gasex}$ tracer, or both. In this study, the residuals are defined as the observations minus the inverse estimates.

[52] The majority of the residuals are generally small relative to the $\Delta C_{gasex}$ signal, but, in some cases, they are quite substantial (Figure S7 of the auxiliary material and Figure 7). Over half of the residuals are less than 20% of the $\Delta C_{gasex}$ concentration for all of the models, and over 90% are less than the total $\Delta C_{gasex}$ concentration for all of the models. The standard deviation of the residuals ranges from 15.9 $\mu mol \ kg^{-1}$ for the UL model to 20.6 $\mu mol \ kg^{-1}$ for the MIT model, while the range of $\Delta C_{gasex}$ estimates is 300 $\mu mol \ kg^{-1}$. The models with the highest radiocarbon skill scores also tend to have lower globally averaged residuals (Table 1 and Figure S6 of the auxiliary material), which suggests that larger residuals are related to deficiencies in the OGCMs.

[53] Another issue of concern is that there is considerable spatial structure in the residuals that is common to all of the models (Figure 7). This spatial structure indicates that the inversion underestimates the spatial gradients that drive the striking pattern of outgassing in the Southern Ocean and uptake at southern midlatitudes found in the inverse estimates. All of the models have positive residuals between 20°S and 40°S in waters shallower than 500 m, and the greatest negative residuals occur in the SAMW (Figure 7). A similar spatial structure is also found in the residuals between observed and modeled temperature and salinity fields, for example, Figure S9 of the auxiliary material
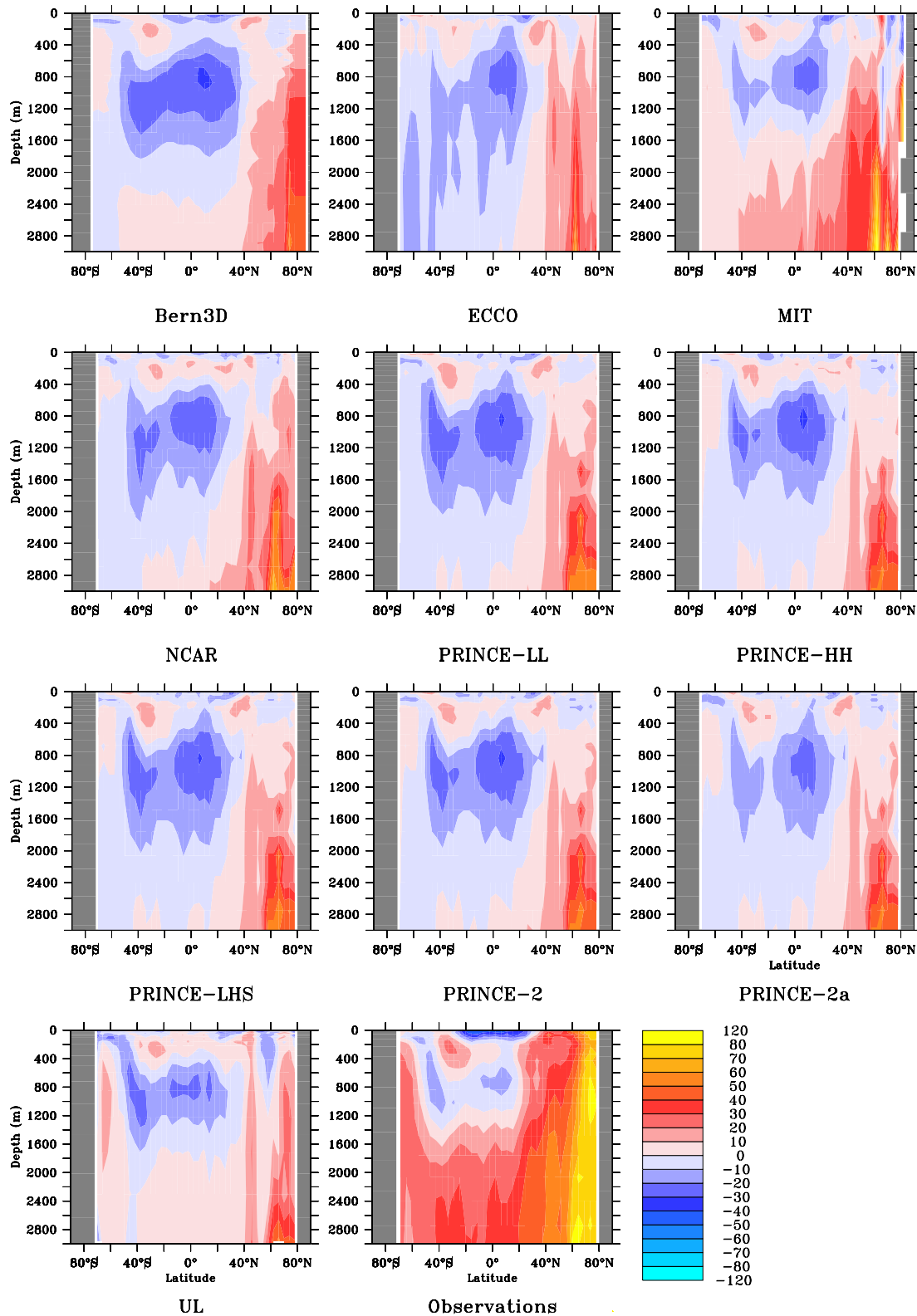
**Figure 7.** Meridional section of the global zonal mean of the difference between the observed $\Delta C_{gasex}$ estimates (bottom row, middle) and the inverse $\Delta C_{gasex}$ estimates for the 10 models that participated in this study (top left through bottom right plots). All plots are in $\mu$mol kg$^{-1}$. Gray areas represent locations where no observations are available or that are outside the model grid. The residuals are defined as the observations minus the inverse estimates. There is relatively little spatial structure in the residuals below 3000 m.

**Table 2.** Summary of the Scenarios Used to Test Hypotheses for Biases in the $r_{C:P}$ and $r_{N:P}$ Ratios Used to Estimate $\Delta C_{gasex}$

| Scenario | Hypothesis | $r_{C:P}$ | $r_{N:P}$ |
|---|---|---|---|
| S$_0$ | ratios from *Anderson and Sarmiento* [1994] (default) | 117 | 14 |
| S$_1$ | low $r_{C:P}$ and $r_{N:P}$ | 102 | 13 |
| S$_2$ | high $r_{C:P}$ and $r_{N:P}$ | 132 | 15 |
| S$_3$ | depth dependent $r_{C:P}$ | 90 (surface)−127 (deep) | 14 |
| S$_4$ | low $r_{C:P}$ south of the Polar front; S$_0$ elsewhere | 91.4 | 13 |
| S$_5$ | low $r_{C:P}$ for waters recently in contact with the surface of the Southern Ocean; S$_0$ elsewhere | 91.4−117 | 13−14 |

[*Doney et al.*, 2004], suggesting that this may be the result of errors in model transport that exist in all of the OGCMs and therefore are not included in our error estimates. The OGCM water masses are generally too cool and too fresh at Southern Hemisphere midlatitudes between about 500 m and 1500 m, which suggests insufficient SAMW formation rates. Therefore the basis functions corresponding to the regions where SAMW is formed may have spatial footprints in the ocean interior that are too diffuse in this water mass. Comparison between the residuals and the basis functions for these regions show that the inversion would not be able to match the low $\Delta C_{gasex}$ values observed in this water mass without incurring even larger residuals in other regions (Figure S8 of the auxiliary material). A recently developed advection scheme has been shown to perform substantially better with regard to formation and preservation of inter-mediate and mode waters than the schemes employed by the OGCMs participating in this study [*Hofmann and Morales Maqueda*, 2006]. Revisiting the ocean inversion with an OGCM using this advection scheme might alleviate some of the spatial structures in the residuals.

[54] In addition, all of the models find substantial positive residuals in the deep ocean at northern high latitudes (Figure 7). This suggests that the OGCMs have insufficient NADW formation and therefore the inversion is unable to match the high observed values in the deep North Atlantic.

[55] These spatially coherent residuals might also be the result of biases in $\Delta C_{gasex}$. For example, a number of studies have suggested that the $r_{C:P}$ ratios south of the Polar Front may be substantially lower than we assumed owing to the prevalence of diatoms in this region [*de Baar et al.*, 1997; *Rubin et al.*, 1998; *Rubin*, 2003]. This would lead to an overestimate of the biological signal that is removed from the observed *DIC*, and therefore to an underestimate of $\Delta C_{gasex}$ (equation (1)). The regions where these low $r_{C:P}$ ratios have been observed play a major role in SAMW formation; therefore this signal would be observed in SAMW. This hypothesis will be tested in the following section.

### 4.2. Sensitivity to Errors in the $\Delta C_{gasex}$

[56] The largest potential sources of error in $\Delta C_{gasex}$ are the $r_{C:P}$ and $r_{N:P}$ stoichiometric ratios used to remove the effect of biology. The uncertainties associated with the observed *DIC*, PO$_4^{3-}$, and *Alk* concentrations (equation (1)) are thought to be relatively small, because careful work has been done to correct for biases between different cruises

[*Key et al.*, 2004], and the data from the historical cruises have been shown to be of comparable quality to the WOCE cruises [*Tanhua and Wallace*, 2005]. The anthropogenic carbon estimates may also be biased [e.g., *Matsumoto and Gruber*, 2005]. Nevertheless, these are expected to have a relatively small impact on $\Delta C_{gasex}$, because the anthropogenic carbon estimates are generally substantially smaller than the biological terms in Equation 1 except in surface waters. We employ a suite of nine scenarios to assess the sensitivity of the inversion to biases in $\Delta C_{gasex}$, consisting of six scenarios to test the sensitivity to biases in the $r_{C:P}$ and $r_{N:P}$ ratios, summarized in Table 2, and three to test the sensitivity to biases in the anthropogenic carbon estimates. These scenarios have been tested using the PRINCE-2, NCAR, and ECCO models with similar results, but we show only results from the PRINCE-2 model in the interest of clarity.

[57] In order to test the sensitivity of the inversion to spatially uniform biases in $r_{C:P}$ and $r_{N:P}$, we recalculated $\Delta C_{gasex}$ using the low (S$_1$) and high (S$_2$) estimates based on the error estimates given by *Anderson and Sarmiento* [1994]. These globally uniform shifts have little effect on the spatial pattern of the air-sea flux estimates of natural CO$_2$ (Figure 8).

[58] Several recent studies have suggested a depth dependence for stoichiometric ratios in the ocean [*Schneider et al.*, 2003, 2004; *Hupe and Karstensen*, 2000]. In order to quantify the effect of such a depth-dependent bias, we recalculated $\Delta C_{gasex}$ using a polynomial fit to the $r_{C:P}$ and $r_{N:P}$ ratios reported by *Hupe and Karstensen* [2000], S$_3$. We chose Hupe and Karstensen's ratios over those of Schneider et al., because the vertical gradients in are larger, permitting us to place some bounds on the largest expected impact of depth-variable ratios.

[59] Scenario S$_3$ leads to less outgassing or more uptake for regions that ventilate the deep ocean, where the $r_{C:P}$ and $r_{N:P}$ ratios are higher and therefore $\Delta C_{gasex}$ is lower compared to the standard scenario, S$_0$. Most notably, the region south of 59°S becomes a substantial sink of natural CO$_2$ and the source is reduced from 0.45 to 0.20 Pg C yr$^{-1}$ in the regions between 44°S and 59°S. The cross-model range for the 44°S to 59°S latitude band is 0.21 to 0.60 Pg C yr$^{-1}$, which suggests that the sensitivity of this region to depth-dependent biases in $\Delta C_{gasex}$ is comparable to the sensitivity to the transport uncertainty. Scenario S$_3$ has more outgassing or less uptake in regions that ventilate shallower waters, particularly in the tropics, where the
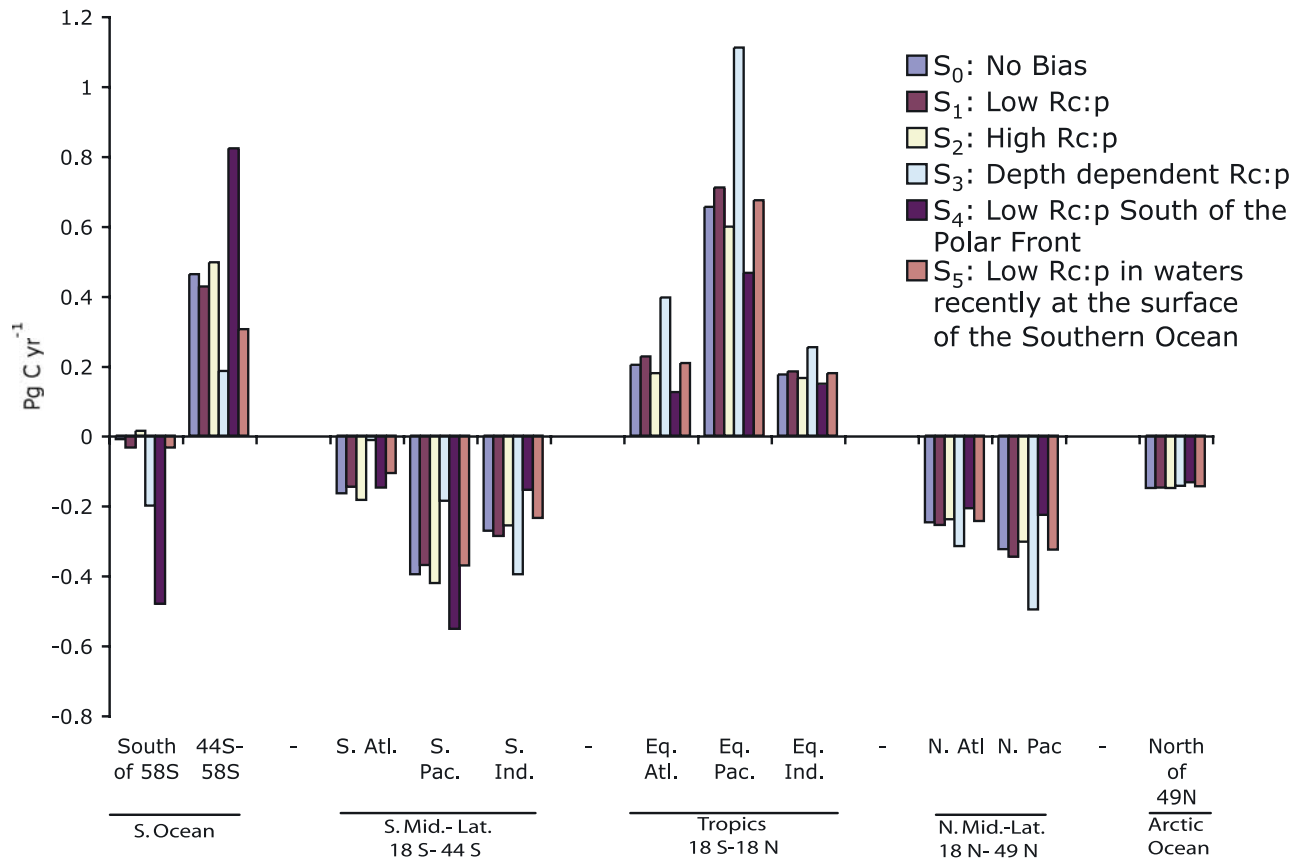
**Figure 8.** Sensitivity of the inverse estimates of the natural $CO_2$ flux (Pg C $yr^{-1}$) to errors in $\Delta C_{gasex}$. The different estimates represent a series of different scenarios for biases in the $r_{C:P}$ and $r_{N:P}$ ratios that are used to remove the influence of ocean interior biology from the observed *DIC* (equation (1)), described in section 4.2. All estimates use the PRINCE-2 OGCM and are aggregated to 11 regions for clarity.

sensitivity to this bias is substantially greater than the sensitivity to model transport. It needs to be noted, however, that the strong depth dependence of the *Hupe and Karstensen*'s [2000] ratios for the Arabian Sea has not been found in any of the many other studies that attempted to estimate stoichiometric ratios of remineralization. Therefore this scenario has to be viewed as extreme.

[60] Low $r_{C:P}$ and $r_{N:P}$ ratios have been observed in the Southern Ocean owing to excess phosphate uptake by diatoms [*de Baar et al.*, 1997; *Rubin et al.*, 1998; *Rubin*, 2003], although *Sweeney et al.* [2003] suggested that this might be a seasonal effect counterbalanced by species that take up far less phosphate in autumn. The low stoichiometric ratios near the surface due to diatoms can be propagated into the interior ocean through sinking *POM* or through mixing or transport of dissolved organic matter (*DOM*) into the interior ocean. The Southern Ocean is a region of low *DOM* production, resulting in a low ratio of *DOM* to *POM* export; therefore the first mechanism is likely to be dominant. Nevertheless, we have constructed scenarios to address each of these mechanisms.

[61] In the first of these scenarios, $S_4$ we set $r_{C:P}$ and $r_{N:P}$ to the values observed by *Rubin et al.* [1998] everywhere

south of the Antarctic Polar Front [*Moore et al.*, 1999], as *Rubin* [2003] observed that the ratios return to values similar to those of *Anderson and Sarmiento* [1994] north of the Polar Front. This approximates the effect of sinking *POM* distributing the low $r_{C:P}$ and $r_{N:P}$ through the thermocline. Scenario $S_4$ leads to a substantial increase in the uptake of natural $CO_2$ south of 59°S and increase in outgassing between 44°S and 59°S, but has little effect on the net outgassing of all these waters south of 44°S, which we base many of our important conclusions on (Figure 8). North of 44°N, the inversion is generally less sensitive to this scenario than to the depth-dependent scenario, although the inverse estimates are generally more sensitive to this scenario than to the choice of OGCM.

[62] In order to approximate the effect of mixing *DOM* with low stoichiometric ratios from the Southern Ocean surface waters into the interior, salinity is used as a tracer. We construct scenario $S_5$ by assigning the *Anderson and Sarmiento* [1994] values to all waters north of 20°S as well as those saltier than 34.4, and linearly interpolating between them. Scenario $S_5$ leads to a 0.15 Pg C $yr^{-1}$ reduction in Southern Ocean (44°S to 59°S) outgassing and nonsignificant changes elsewhere (Figure 8).

[63] The effects of biases in the anthropogenic carbon estimates were tested using the same scenarios described by *Mikaloff Fletcher et al.* [2006]: a globally uniform low and high estimate of the stoichiometric $r_{C:O}$ ratio used in the anthropogenic carbon calculation and a hypothetical depth-dependent bias similar to the findings of *Matsumoto and Gruber* [2005]. We find that the natural flux estimates are insensitive to biases in the anthropogenic carbon estimates (Figure S10 of the auxiliary material), in agreement with *Jacobson et al.* [2007b].

[64] The differences between the flux estimates for these scenarios are generally less than 0.01 Pg C yr$^{-1}$ except for the Southern Ocean south of 59°S, where the difference is less than 0.03 Pg C yr$^{-1}$.

[65] Overall, we find that the results tend to be more sensitive to biases in $\Delta C_{gasex}$ than to the choice of OGCM. The Southern Ocean is the most sensitive to these biases, however none of the relatively extreme scenarios tested here remove the spatial pattern of substantial outgassing south of 59°S and uptake between 44°S and 50°S.

## 5. Conclusions

[66] We find an overall spatial pattern of substantial natural CO$_2$ uptake at midlatitudes of both the Northern and Southern Hemispheres and considerable outgassing in the tropics and south of 44°S. This spatial pattern of sources and sinks differs considerably from many previous forward simulations, including OCMIP-2, in the Southern Hemisphere south of 20°S [*Murnane et al.*, 1999; *Sarmiento et al.*, 2000; *Watson and Orr*, 2003; *Wetzel et al.*, 2005]. However, it is in better agreement with some more recent forward simulations with more complex ecological/biogeochemical models [*Moore et al.*, 2004; *Doney et al.*, 2006].

[67] We have a substantial level of confidence in these results, because the inverse flux estimates correspond to spatial gradients in $\Delta C_{gasex}$ and are remarkably insensitive to the choice of OGCM. While the inverse estimates in the Southern Ocean are sensitive to potential biases in $\Delta C_{gasex}$, the overall spatial structure of outgassing between 59°S and 44°S and uptake between 44°S and 18°S persists in all of the relatively extreme scenarios that we explored. Although we have undertaken extensive error analysis, the errors in this study do not account for the possibility of unquantified errors due to variability in ocean transport or errors in the ocean transport common to all of the models. The residuals between the data-based $\Delta C_{gasex}$ estimates and the models suggest there may be some errors in transport common to all of the models, a shortcoming that needs to be revised with the next generation of OGCMs.

[68] Our findings in the Southern Hemisphere have significant implications for the past, present, and future carbon cycle. For example, several groups have hypothesized that the low atmospheric CO$_2$ concentrations during the ice ages may be related to biogeochemical changes in the Southern Ocean [*Sigman and Boyle*, 2000]. These authors argue that upwelling of *DIC*-rich waters in the Southern Ocean combined with an inefficient biological pump lead to outgassing of CO$_2$ from this region during interglacial periods. During glacial times, they suggested that this natural CO$_2$ source was damped owing to increased nutrient utilization or decreased ventilation of deep waters as a result of increased stratification [*Toggweiler*, 1999]. We find a large natural outgassing of CO$_2$, which supports the hypothesis of substantial Southern Ocean outgassing during interglacial periods and confirms the potential sensitivity of this region to climate changes.

[69] *Jacobson et al.* [2007b] found a substantial contemporary terrestrial source in the Southern Hemisphere using an atmospheric inversion that was coupled to an ocean inversion for fluxes of both anthropogenic and natural CO$_2$. This tropical land source implies that a large tropical CO$_2$ fertilization sink on land is not needed to close the CO$_2$ budget. The terrestrial results for the Southern Hemisphere in this study were closely linked to the finding of a very large natural and anthropogenic CO$_2$ sink in the midlatitude Southern Hemisphere ocean and a substantial natural CO$_2$ source in the Southern Ocean.

[70] A third implication is that simulations using ocean carbon cycle models have suggested that future climate warming could lead to less anthropogenic CO$_2$ uptake in the Southern Ocean as a result of increased stratification and therefore decreased ventilation of deep waters in this region [*Sarmiento et al.*, 1998]. Increased stratification might also lead to a decrease in the large natural Southern Ocean outgassing found in this study, because it would reduce the upwelling of *DIC*-rich deep waters in this region, and therefore reduce the natural CO$_2$ outgassing, which would more than compensate for reduced biological uptake [*Fung et al.*, 2005; *Doney et al.*, 2006]. This implies that the decreased anthropogenic carbon uptake in the Southern Ocean could be largely balanced by a reduction in outgassing of natural carbon, making an accurate projection of the possible oceanic feedbacks in a changing climate challenging.

## References

Álvarez, M., A. Ríos, F. F. Pérez, H. L. Bryden, and G. Rosón (2003), Transports and budgets of total inorganic carbon in the subpolar and temperate North Atlantic, *Global Biogeochem. Cycles*, *17*(1), 1002, doi:10.1029/2002GB001881.

Anderson, L. A., and J. L. Sarmiento (1994), Redfield ratios of remineralization determined by nutrient data analysis, *Global Biogeochem. Cycles*, *8*(1), 65–80.

Bousquet, P., P. Peylin, P. Ciais, C. LeQuéré, P. Friedlingstein, and P. P. Tans (2000), Regional changes in carbon dioxide fluxes of land and oceans since 1980, *Science*, *290*, 1342–1346.

Brewer, P. G., C. Goyet, and D. Dyrssen (1989), Carbon dioxide transport by ocean currents at 25°N latitude in the Atlantic Ocean, *Science*, *246*, 477–479.

Broecker, W. S., and T.-H. Peng (1992), Interhemispheric transport of carbon dioxide by ocean circulation, *Nature*, *356*, 587–589.

Bryden, H. L., E. L. McDonagh, and B. A. King (2003), Changes in ocean water mass properties: Oscillations or trends?, *Science*, *300*, 2086–2088.

Caldeira, K., and P. B. Duffy (2000), The role of the Southern Ocean in uptake and storage of anthropogenic carbon dioxide, *Science*, *287*, 620–622.

da Silva, A. M., C. C. Young, and S. Levitus (1994), *Atlas of Surface Marine Data 1994*, vol. 1, *Algorithms and Procedures*, NOAA Atlas NESDIS 6, Natl. Oceanic and Atmos. Admin., Silver Spring, Md.

de Baar, H. J. W., M. A. V. Leeuwe, R. Scharek, L. Goeyens, K. M. J. Bakker, and P. Fritsche (1997), Nutrient anomalies in Fragilariopsis Kerguelensis blooms, iron deficiency and the nitrate/phosphate ratio (A. C. Redfield) of the Antarctic Ocean, *Deep Sea Res., Part II*, *44*, 229–260.

Doney, S. C., J. L. Bullister, and R. Wanninkhof (1998), Climatic variability in upper ocean ventilation rates diagnosed using chlorofluorocarbons, *Geophys. Res. Lett.*, *25*(9), 1399–1402.

Doney, S., et al. (2004), Evaluating global ocean carbon models: The importance of realistic physics, *Global Biogeochem. Cycles*, *18*, GB3017, doi:10.1029/2003GB002150.

Doney, S. C., K. Lindsay, I. Fung, and J. John (2006), Natural variability in a stable 1000 year coupled climate-carbon simulation, *J. Clim.*, *19*(13), 3033–3054.

Dutay, J.-C., et al. (2002), Evaluation of ocean model ventilation with CFC-11: Comparison of 13 global ocean models, *Ocean Modell.*, *4*, 89–120.

Enting, I. G., and J. V. Mansbridge (1989), Latitudinal distribution of sources and sinks of atmospheric CO$_2$: Direct inversion of filtered data, *Tellus, Ser. B.*, *41*, 111–126.

Fung, I. Y., S. C. Doney, K. Lindsay, and J. John (2005), Evolution of carbon sinks in a changing climate, *Proc. Natl. Acad. Sci. U. S. A.*, *202*, 11,201–11,206, doi:10.1073/pnas.0504949102.

García, M., I. Bladé, A. Cruzado, Z. Velásquez, H. García, J. Puigdefabregas, and J. Sospedra (2002), Observed variability of water properties and transports on the World Ocean Circulation Experiment SR1b section across the Antarctic Circumpolar Current, *J. Geophys. Res.*, *107*(C10), 3162, doi:10.1029/2000JC000277.

Gloor, M., N. Gruber, T. M. C. Hughes, and J. L. Sarmiento (2001), An inverse modeling method for estimation of net air-sea fluxes from bulk data: Methodology and application to the heat cycle, *Global Biogeochem. Cycles*, *15*(4), 767–782.

Gloor, M., N. Gruber, J. L. Sarmiento, C. L. Sabine, R. A. Feely, and C. Roedenbeck (2003), A first estimate of present and pre-industrial air-sea CO$_2$ fluxes patterns based on ocean interior carbon measurements and models, *Geophys. Res. Lett.*, *30*(1), 1010, doi:10.1029/2002GL015594.

Gnanadesikan, A., N. Gruber, R. D. Slater, and J. L. Sarmiento (2002), Oceanic vertical exchange and new production: A comparison between model results and observations, *Deep Sea Res., Part II*, *49*, 363–401.

Gnanadesikan, A., J. P. Dunne, R. M. Key, K. Matsumoto, J. L. Sarmiento, R. D. Slater, and P. S. Swathi (2004), Oceanic ventilation and biogeochemical cycling: Understanding the physical mechanisms that produce realistic distributions of tracers and productivity, *Global Biogeochem. Cycles*, *18*, GB4010, doi:10.1029/2003GB002097.

Gruber, N. (1998), Anthropogenic CO$_2$ in the Atlantic Ocean, *Global Biogeochem. Cycles*, *12*(1), 165–191.

Gruber, N. and J. L. Sarmiento (2002), Biogeochemical/physical interactions in elemental cycles, in *The Sea: Biological-Physical Interactions in the Oceans*, vol. 12, edited by A. R. Robinson, J. J. McCarthy, and B. J. Rothschild, pp. 337–399, John Wiley, Hoboken, N. J.

Gruber, N., J. L. Sarmiento, and T. F. Stocker (1996), An improved method for detecting anthropogenic CO$_2$ in the oceans, *Global Biogeochem. Cycles*, *10*(4), 809–837.

Gruber, N., M. Gloor, T. M. C. Hughes, and J. L. Sarmiento (2001), Air-sea flux of oxygen estimated from bulk data: Implications for the marine and atmospheric oxygen cycle, *Global Biogeochem. Cycles*, *15*(4), 783–803.

Gruber, N., P. Friedlingstein, C. B. Field, R. Valentini, M. Heimann, J. E. Richey, P. Romero-Lankao, D. Schulze, and C. Chen (2004), The vulnerability of the carbon cycle in the 21st century: An assessment of carbon-climate-human interactions, in *The Global Carbon Cycle: Integrating Humans, Climate, and the Natural World*, edited by C. B. Field and M. R. Raupach, chap. 2, pp. 45–76, Island, Washington, D. C.

Gurney, K. R., et al. (2002), Towards robust regional estimates of CO$_2$ sources and sinks using atmospheric transport models, *Nature*, *415*, 626–630.

Hofmann, M., and M. A. Morales Maqueda (2006), Performance of a second-order moments advection scheme in an Ocean General Circulation Model, *J. Geophys. Res.*, *111*, C05006, doi:10.1029/2005JC003279.

Holfort, J., K. M. Johnson, B. Siedler, and D. W. R. Wallace (1998), Meridional transport of dissolved inorganic carbon in the South Atlantic Ocean, *Global Biogeochem. Cycles*, *12*(3), 479–499.

Hupe, A., and J. Karstensen (2000), Redfield stoichiometry in Arabian Sea subsurface waters, *Global Biogeochem. Cycles*, *14*(1), 357–372.

Jacobson, A. R., et al. (2007a), A joint atmosphere-ocean inversion for surface fluxes of carbon dioxide: 1. Methods, *Global Biogeochem. Cycles*, doi:10.1029/2005GB002556, in press.

Jacobson, A. R., et al. (2007b), A joint atmosphere-ocean inversion for surface fluxes of carbon dioxide: 2. Results, *Global Biogeochem. Cycles*, doi:10.1029/2006GB002703, in press.

Johnson, G. C., and N. Gruber (2007), Water mass variations along 20°W in the Northeastern Atlantic Ocean, *Progr. Oceanogr.*, in press.

Joos, F., G.-K. Plattner, T. F. Stocker, O. Marchal, and A. Schmittner (1999), Global warming and marine carbon cycle feedbacks on future atmospheric CO$_2$, *Science*, *284*, 464–467.

Kaminski, T., P. J. Rayner, M. Heimann, and I. G. Enting (2001), On aggregation errors in atmospheric transport inversions, *J. Geophys. Res.*, *106*(D5), 4703–4716.

Keeling, C. D., R. B. Bacastow, A. F. Carter, S. C. Piper, T. P. Whorf, M. Heimann, W. G. Mook, and H. Roeloffzen (1989a), A three-dimensional model of atmospheric CO$_2$ transport based on observed winds: 1. Analysis of observational data, in *Aspects of Climate Variability in the Pacific and the Western Americas*, *Geophys. Monogr. Ser.*, vol. 55, edited by D. H. Peterson, pp. 165–237, AGU, Washington, D. C.

Keeling, C. D., S. C. Piper, and M. Heimann (1989b), A three-dimensional model of atmospheric CO$_2$ transport based on observed winds: 4. Mean annual gradients and interannual variations, in *Aspects of Climate Variability in the Pacific and the Western Americas*, *Geophys. Monogr. Ser.*, vol. 55, edited by D. H. Peterson, pp. 305–363, AGU, Washington, D. C.

Keeling, R. F., and T.-H. Peng (1995), Transport of heat, CO$_2$ and O$_2$ by the Atlantic's thermohaline circulation, *Philos. Trans. R. Soc., Ser. B*, *348*, 133–142.

Key, R. M., et al. (2004), A global ocean carbon climatology: Results from Global Data Analysis Project (GLODAP), *Global Biogeochem. Cycles*, *18*, GB4031, doi:10.1029/2004GB002247.

Lerman, A., F. Mackenzie, and L. M. Ver (2004), Coupling of the perturbed C-N-P cycles in industrial time, *Aquat. Geochem.*, *10*, 3–32.

Levitus, S., J. I. Antonov, T. P. Boyer, and C. Stephens (2000), Warming of the World Ocean, *Science*, *287*, 2225–2229.

Lundberg, L., and P. M. Haugan (1996), A nordic seas-arctic ocean carbon budget from volume flows and inorganic carbon data, *Global Biogeochem. Cycles*, *10*(3), 493–510.

Macdonald, A. M., M. O. Baringer, R. Wanninkhof, K. Lee, and D. W. R. Wallace (2003), A 1998–1992 comparison of inorganic carbon and its transport across 24.5°N in the Atlantic, *Deep Sea Res., Part II*, *50*, 3041–3064.

Matear, R. J., and A. C. Hirst (1999), Climate change feedback on the future oceanic CO$_2$ uptake, *Tellus, Ser. B.*, *51*, 722–733.

Matsumoto, K., and N. Gruber (2005), How accurate is the estimation of anthropogenic carbon in the ocean?, *Global Biogeochem. Cycles*, *19*, GB3014, doi:10.1029/2004GB002397.

Matsumoto, K., et al. (2004), Evaluation of ocean carbon cycle models with data-based metrics, *Geophys. Res. Lett.*, *31*, L07303, doi:10.1029/2003GL018970.

McPhaden, M. J., and D. Zhang (2002), Slowdown of the meridional overturning circulation in the upper Pacific Ocean, *Nature*, *415*, 603–608.

Mikaloff Fletcher, S. E., N. P. Gruber, and A. Jacobson (2003), Ocean Inversion Project how-to document version 1.0, report, 18 pp., Inst. for Geophys. and Planet. Phys., Univ. of Calif., Los Angles.

Mikaloff Fletcher, S. E., et al. (2006), Inverse estimates of anthropogenic CO$_2$ uptake, transport, and storage by the ocean, *Global Biogeochem. Cycles*, *20*, GB2002, doi:10.1029/2005GB002530.

Moore, J. K., M. R. Abbott, and J. G. Richman (1999), Location and dynamics of the Antarctic Polar Front from satellite sea surface temperature data, *J. Geophys. Res.*, *104*(C2), 3059–3073.

Moore, J. K., S. C. Doney, and K. Lindsay (2004), Upper ocean ecosystem dynamics and iron cycling in a global three-dimensional model, *Global Biogeochem. Cycles*, *18*, GB4028, doi:10.1029/2004GB002220.

Müller, S. A., F. Joos, N. R. Edwards, and T. F. Stocker (2006), Water mass distribution and ventilation time scales in a cost-efficient, three-dimensional ocean model, *J. Clim.*, *19*(21), 5479–5499.

Murnane, R. J., J. L. Sarmiento, and C. LeQuéré (1999), The spatial distribution of air-sea fluxes and the interhemispheric transport of carbon by the oceans, *Global Biogeochem. Cycles*, *13*(2), 287–305.

Najjar, R. and J. C. Orr (1999), Biotic—HOWTO, internal OCMIP report, Lab. des Sci. du Clim. et de l'Environ., Gif-sur-Yvette, France.

Orr, J. C., R. Najjar, C. L. Sabine, and F. Joos (1999), Abiotic—HOWTO, internal OCMIP report, Lab. des Sci. du Clim. et de l'Environ., Gif-sur-Yvette, France.

Plattner, G.-K., F. Joos, T. F. Stocker, and O. Marchal (2001), Feedback mechanisms and sensitivities of ocean carbon uptake under global warming, *Tellus, Ser. B.*, 53, 564–592.

Press, W., S. Teukolsky, W. Vetterling, and B. Flannery (1992), *Numerical Recipes*, 2nd ed., Cambridge Univ. Press, New York.

Rosón, G., A. F. Ríos, F. F. Pérez, A. Lavin, and H. L. Bryden (2003), Carbon distribution, fluxes, and budgets in the subtropical North Atlantic Ocean (24.5°N), *J. Geophys. Res.*, 108(C5), 3144, doi:10.1029/1999JC000047.

Rubin, S. I. (2003), Carbon and nutrient cycling in the upper water column across the Polar Frontal Zone and Antarctic Circumpolar Current along 170 W, *Global Biogeochem. Cycles*, 17(3), 1087, doi:10.1029/2002GB001900.

Rubin, S. I., T. Takahashi, D. W. Chipman, and J. G. Goddard (1998), Primary productivity and nutrient utilization ratios in the Pacific sector of the Southern Ocean based on seasonal changes in seawater chemistry, *Deep Sea Res., Part I*, 45, 1211–1234.

Sarmiento, J. L., and E. T. Sundquist (1992), Revised budget for the oceanic uptake of anthropogenic carbon dioxide, *Nature*, 356, 589–593.

Sarmiento, J. L., J. C. Orr, and U. Siegenthaler (1992), A perturbation simulation of $CO_2$ uptake in an ocean general circulation model, *J. Geophys. Res.*, 97(C3), 3621–3645.

Sarmiento, J. L., T. M. C. Hughes, R. J. Stouffer, and S. Manabe (1998), Simulated response of the ocean carbon cycle to anthropogenic climate warming, *Nature*, 393, 245–249.

Sarmiento, J. L., P. Monfray, E. Maier-Reimer, O. Aumont, R. Murnane, and J. Orr (2000), Sea-air $CO_2$ fluxes and carbon transport: A comparison of three ocean general circulation models, *Global Biogeochem. Cycles*, 14(4), 1267–1281.

Schneider, B., R. Schlitzer, and G. Fischer (2003), Depth-dependent elemental compositions of particulate organic matter (POM) in the ocean, *Global Biogeochem. Cycles*, 17(2), 1032, doi:10.1029/2002GB001871.

Schneider, B., A. Engel, and R. Schlitzer (2004), Effects of depth-dependent C:N ratios of particulate organic matter (POM) on the marine carbon cycle, *Global Biogeochem. Cycles*, 18, GB2015, doi:10.1029/2003GB002184.

Sigman, D. M., and E. A. Boyle (2000), Glacial/interglacial variations in atmospheric carbon dioxide, *Nature*, 407, 859–869.

Stoll, M. H. C., H. M. van Aken, H. J. W. de Baar, and C. J. de Boer (1996), Meridional carbon dioxide transport in the northern North Atlantic, *Mar. Chem.*, 55, 205–216.

Sweeney, E. N., D. J. McGillicuddy, and K. O. Buesseler (2003), Biogeochemical impacts due to mesoscale eddy activity in the Sargasso Sea as measured at the Bermuda Atlantic Time-series Study (BATS), *Deep Sea Res., Part II*, 50, 3017–3039.

Takahashi, T., et al. (2002), Global sea-air $CO_2$ flux based on climatological surface ocean pCO₂, and seasonal biological and temperature effects, *Deep Sea Res., Part II*, 49, 1601–1622.

Tanhua, T., and D. W. R. Wallace (2005), Consistency of TTO-NAS inorganic carbon data with modern measurements, *Geophys. Res. Lett.*, 32, L14618, doi:10.1029/2005GL023248.

Tans, P. P., I. Y. Fung, and T. Takahashi (1990), Observational constraints on the global atmospheric $CO_2$ budget, *Science*, 247, 1431–1438.

Taylor, K. E. (2001), Summarizing multiple aspects of model performance in a single diagram, *J. Geophys. Res.*, 106(D7), 7183–7192.

Toggweiler, J. R. (1999), Variations of atmospheric $CO_2$ driven by ventilation of the ocean's deepest water, *Paleoceanography*, 14(5), 571–588.

Wallace, D. R. (2001), Storage and transport of excess $CO_2$ in the oceans: The JGOFS/WOCE Global $CO_2$ Survey, in *Ocean Circulation and Climate*, pp. 489–521, Elsevier, New York.

Watson, A. J., and J. C. Orr (2003), Carbon dioxide fluxes in the global ocean, in *Ocean Biogeochemistry*, pp. 123–143, Springer, New York.

Wetzel, P., A. Winguth, and E. Maier-Reimer (2005), Sea-to-air $CO_2$ flux from 1948 to 2003: A model study, *Global Biogeochem. Cycles*, 19, GB2005, doi:10.1029/2004GB002339.

————————————

S. Doney, Marine Chemistry and Geochemistry, MS 25, Woods Hole Oceanographic Institution, 360 Woods Hole Road, Woods Hole, MA 02543-1543, USA. (sdoney@whoi.edu)

S. Dutkiewicz and M. Follows, Department of Earth, Atmosphere, and Planetary Sciences, Massachusetts Institute of Technology, 54-1412, 77 Massachusetts Avenue, Cambridge, MA 02139, USA. (stephd@ocean.mit.edu; mick@ocean.mit.edu)

M. Gerber, S. A. Müller, and F. Joos, Climate and Environmental Physics, Physics Institute, University of Bern, Sidlerstr. 5, CH-3012 Bern, Switzerland. (mgerber@climate.unibe.ch; smueller@climate.unibe.ch; joos@climate.unibe.ch)

M. Gloor, Institutes of Earth and Biosphere, Energy and Environment and School of Geography, University of Leeds, Leeds, UK. (e.gloor@leeds.ac.uk)

N. Gruber, Environmental Physics, Institute of Biochemistry and Pollutant Dynamics, ETH Zürich, CHN E21.1, CH-8092 Zürich, Switzerland. (nicolas.gruber@env.ethz.ch)

A. R. Jacobson, NOAA Earth System Research Laboratory, Global Monitoring Division, 325 Broadway, Boulder, CO 80305, USA. (andy.jacobson@noaa.gov)

K. Lindsay, Climate and Global Dynamics, National Center for Atmospheric Research, P.O. Box 3000, Boulder, CO 80307, USA. (klindsay@ucar.edu)

D. Menemenlis, Estimating the Circulation and Climate of the Ocean, Jet Propulsion Laboratory, MS 300-323, 4800 Oak Grove Drive, Pasadena, CA 91109, USA. (menemenlis@jpl.nasa.gov)

S. E. Mikaloff Fletcher and J. Sarmiento, Program in Atmospheric and Oceanic Sciences, Princeton University, PO Box CN710, Princeton, NJ 08544-0710, USA. (mikaloff@princeton.edu; jls@princeton.edu)

A. Mouchet, Astrophysics and Geophysics Institute, University of Liege, Allée du 6 Août, 17 Bt. B5c, B-4000 Liege, Belgium. (a.mouchet@ulg.ac.be)